



22 **Abstract**

23 The next-generation National Air Quality Forecast Capability (NAQFC) will use
24 the meteorology from Global Forecast System with the new Finite Volume Cube-Sphere
25 dynamic core (GFS-FV3) to drive the chemical evolution of gases and particles described
26 by the Community Multiscale Air Quality modelling system version 5.3 (CMAQ v5.3).
27 CMAQ v5.0.2, a historical version of CMAQ, has been coupled with the North American
28 Mesoscale Forecast System (NAM) model in the current operational NAQFC. An
29 experimental version of the NAQFC based on the offline-coupled GFS-FV3 version 15
30 with CMAQv5.0.2 modeling system (GFSv15-CMAQv5.0.2), has been developed by the
31 National Oceanic and Atmospheric Administration (NOAA) to provide real-time air
32 quality forecasts over the contiguous United States (CONUS) since 2018. In this work,
33 comprehensive region-specific, time-specific, and categorical evaluations are conducted
34 for meteorological and chemical forecasts from the offline-coupled
35 GFSv15-CMAQv5.0.2 for the year 2019. The forecast system shows good overall
36 performance in forecasting meteorological variables with the annual mean biases of
37 -0.2 °C for temperature at 2-m, 0.4% for relative humidity at 2-m, and 0.4 m s⁻¹ for wind
38 speed at 10-m against the METeorological Aerodrome Reports (METAR) dataset. Larger
39 biases occur in seasonal and monthly mean forecasts, particularly in spring. Although the
40 monthly accumulated precipitation forecasts show generally consistent spatial
41 distributions with those from the remote sensing and ensemble datasets,



42 moderate-to-large biases exist in hourly precipitation forecasts against the Clean Air
43 Status and Trends Network (CASTNET) and METAR. While the forecast system
44 performs well in forecasting ozone (O_3) throughout the year and fine particles with a
45 diameter of $2.5\ \mu\text{m}$ or less ($PM_{2.5}$) for warm months (May-September), it significantly
46 overpredicts annual-mean concentrations of $PM_{2.5}$. This is due mainly to the high
47 predicted concentrations of fine fugitive, coarse-mode, and nitrate particle components.
48 Underpredictions in the southeastern U.S. and California during summer are attributed to
49 missing sources and mechanisms of secondary organic aerosol formation from biogenic
50 volatile organic compounds (VOCs) and semi- or intermediate-VOCs. This work
51 identifies possible underlying causes for systematic region- and time-specific model
52 biases, which will provide a scientific basis for further development of the
53 next-generation NAQFC, in particular, derivation of the science-based bias correction
54 methods to improve forecasting skill for O_3 and $PM_{2.5}$.

55

56 **1. Introduction**

57 Three-dimensional air quality models (3-D AQMs) have been widely applied in
58 real time air quality forecasting (RT-AQF) since the 1990s in the U.S. (Stein et al., 2000;
59 McHenry et al., 2004; Zhang et al., 2012a). The developments and applications of the
60 national air quality forecasting systems based on 3-D AQMs were conducted in the 2000s
61 (Kang et al., 2005; Otte et al., 2005; McKeen et al., 2005, 2007, 2009). Since then,



62 improvements and significant progress have been achieved in RT-AQF through the
63 further development of AQMs and the use of advanced techniques. For example, more air
64 pollutants in the products, more detailed gas-phase chemical mechanisms and aerosol
65 chemistry, and the implementation of chemical data assimilation were available (Zhang et
66 al., 2012b; Lee et al., 2017). Various AQMs, coupled with meteorological models in
67 either an online or offline manner, were developed and applied in RT-AQF (e.g., Chuang
68 et al., 2011; Lee et al., 2011; Žabkar et al., 2015; Ryan, 2016). The early version of the
69 National Air Quality Forecast Capability (NAQFC) was jointly developed by the U.S.
70 National Oceanic and Atmospheric Administration (NOAA) and the U.S. Environmental
71 Protection Agency (EPA) to provide forecasts of ozone (O_3) over the northeastern U.S.
72 (Eder et al., 2006). Since the first operational version over the contiguous United States
73 (CONUS) (Eder et al., 2009), the NAQFC has been continuously updated and developed
74 to provide more forecasting products (including O_3 , smoke, dust, and particulate matter
75 with a diameter of $2.5 \mu\text{m}$ or less ($PM_{2.5}$)) with increasing accuracy (Mathur et al., 2008;
76 Stajner et al., 2011; Lee et al., 2017).

77 The forecast skill of a historical NAQFC, which was based on the North
78 American Mesoscale Forecast System (NAM) model (Black, 1994) and the Community
79 Multiscale Air Quality Modeling System version 4.6 (CMAQ v4.6), over CONUS during
80 year 2008 was evaluated by Kang et al. (2010a) for operational O_3 and experimental
81 $PM_{2.5}$ products. Overall, maximum 8-h O_3 was slightly overpredicted over the CONUS



82 during the summer, with the mean bias (MB), normalized mean bias (NMB), and
83 correlation coefficient (Corr) of 3.2 ppb, 6.8 %, and 0.65, respectively. The performance
84 of predicted daily mean $PM_{2.5}$ varied: with an underprediction during the warm season
85 and an overprediction in the cool season. The MBs and NMBs during warm/cool seasons
86 were $-2.3/4.5 \mu\text{g m}^{-3}$ and $-19.6\%/45.1\%$, respectively. The current version of the U.S.
87 NOAA's operational NAQFC has provided the air quality forecast to the public for O_3
88 and $PM_{2.5}$ at a horizontal grid resolution of 12 km over CONUS since 2015. It is currently
89 based on the CMAQ v5.0.2 (released May 2014) (U.S. EPA, 2014) coupled offline with
90 the NAM model. Daily mean $PM_{2.5}$ was underpredicted during warm months (May and
91 July 2014) and overpredicted during a cool month (January 2015) over CONUS still
92 persist (Lee et al., 2017).

93 Efforts have been made to reduce the seasonal and region-specific biases in the
94 historical and current NAQFC. Development and implementation of an analog ensemble
95 bias correction approach was applied to the operational NAQFC to improve forecast
96 performance in $PM_{2.5}$ predictions (Huang et al., 2017). Kang et al. (2008, 2010)
97 investigated the Kalman Filter (KF) bias-adjustment technique for operational use in the
98 NAQFC system. The KF bias-adjusted forecasts showed significant improvement in both
99 O_3 and $PM_{2.5}$ for discrete and categorical evaluations. However, limitations in the
100 underlying models and the bias correction/adjustment approaches need further
101 improvement. Characterizing the current NAQFC forecasting skill and identifying the



102 underlying causes for region- and time-specific biases can result in further development
103 of the NAQFC system and improved pollutant predictions.

104 In the next generation NAQFC, the NAM will be replaced by the Finite Volume
105 Cube-Sphere Dynamical Core (FV3), the dynamical core in Global Forecast System
106 (GFS). To support this new development, a prototype of the offline-coupled GFS version
107 15 (v15) with CMAQv5.0.2 (GFSv15-CMAQv5.0.2) has been developed and applied by
108 the NOAA for RT-AQF over CONUS since 2018 (Huang et al., 2018, 2019, 2020). In
109 this work, the meteorological and air quality forecasts from the offline-coupled
110 GFSv15-CMAQv5.0.2 are comprehensively evaluated for the year of 2019. The main
111 objectives of this work are to: (1) evaluate the forecast skills of the experimental
112 prototype of the GFSv15-CMAQv5.0.2 system; (2) identify the major model biases, in
113 particular, systematic biases and persistent region- and time-specific biases in major
114 species; (3) investigate underlying causes for the biases to provide a scientific basis for
115 improving the model representations of chemical processes and developing science-based
116 bias correction methods for O₃ and PM_{2.5} forecasts. This work will support NAQFC's
117 further development and improvement through enhancing its forecasting abilities and
118 generating a benchmark for the operational version of next-generation NAQFC that is
119 being developed by NOAA based on the offline-coupled GFS-FV3 v16 with CMAQ v5.3
120 (Campbell et al., 2020). Eventually, the latest version of CMAQ (version 5.3), which has
121 updates in gas-phase chemistry (Yarwood et al., 2010; Emery et al., 2015; Luecken et al.,



122 2019), lightning nitric oxide (LNO) production schemes (Kang et al., 2019a, 2019b), and
123 secondary aerosol formation (in particular, secondary organic aerosol) (e.g., Pye et al.,
124 2013, 2017; Murphy et al., 2017) among others, will be coupled with GFS-FV3 v16 and
125 be implemented into NAQFC.

126

127 **2. Model system and evaluation protocols**

128 2.1 Description and configuration of offline-coupled GFSv15-CMAQv5.0.2

129 FV3 is a dynamical core for atmospheric numerical models developed by the
130 Geophysical Fluid Dynamics Laboratory (GFDL) (Putman and Lin, 2007). It is a modern
131 and extended version of the original FV core with a cubed-sphere grid design and more
132 computationally efficient solvers. It was selected for implementation into the GFS as the
133 next generation dynamical core in 2016 (Zhang et al., 2019a). The GFS-FV3 v15 (GFS
134 v15) has been operational since June 2019. The GFS v15 uses the Rapid Radiative
135 Transfer Method for GCMs (RRTMG) scheme for shortwave/longwave radiation
136 (Mlawer et al., 1997; Iacono et al., 2000; Clough et al., 2005), the Hybrid
137 eddy-diffusivity mass-flux (EDMF) scheme for Planetary Boundary Layer (PBL)
138 (National Centers for Environmental Prediction, 2019a), the Noah Land Surface Model
139 (LSM) scheme for land surface option (Chen et al., 1997), the Simplified
140 Arakawa-Schubert (SAS) deep convection for cumulus parameterization (Arakawa et al.,



141 1974; Grell, 1993), and a more advanced GFDL microphysics scheme for microphysics
142 (National Centers for Environmental Prediction, 2019b). An interface preprocessor has
143 been developed by NOAA to interpolate data, transfer coordinates, and convert the GFS
144 v15 outputs into the data format required by CMAQv5.0.2 (Huang et al., 2018, 2019).
145 The original outputs from GFS v15, which have a horizontal grid with 13-km resolution
146 and a Lagrangian vertical coordinate with 64 layers in NEMSIO format, are processed to
147 Lambert-Conformal Conic projection by PREMAQ, a preprocessor, to recast the
148 meteorological fields for CMAQ into an Arakawa C-staggering grid (Arakawa and Lamb,
149 1977) with a 12-km horizontal resolution and 35 vertical layers (Table 1). The first 72
150 hours in 12:00 UTC forecast cycles from GFS v15 are used to drive the air quality
151 forecast by the offline-coupled GFSv15-CMAQv5.0.2 system.

152 CMAQ has been continuously developed by the U.S. EPA since the 1990s (Byun
153 and Schere, 2006) and has been significantly updated in many atmospheric processes
154 since then. Chemical boundary conditions for the GFSv15-CMAQv5.0.2 system are
155 mainly from the global 3-D model of atmospheric chemistry driven by meteorological
156 input from the Goddard Earth Observing System (GEOS-Chem). The lateral boundary
157 condition for dust is from the outputs of NEMS GFS Aerosol Component (NGAC) (Lu et
158 al., 2016). The area sources from National Emissions Inventory of year 2014 version 2
159 (NEI 2014v2), point sources from NEI 2005 with projected sulfur dioxide (SO₂) and
160 nitrogen oxide (NO_x) to year 2019, and U.S. EPA's MOVES 2014 mobile sources along



161 with the biomass burning emission inventory from the Blended Global Biomass Burning
162 Emissions Product system (GBBEPx) (Zhang et al., 2019b) are processed by Sparse
163 Matrix Operator Kernel Emissions (SMOKE) model and the PREMAQ for CMAQ.
164 Biogenic emissions are calculated inline by Biogenic Emission Inventory System (BEIS)
165 version 3.14 (Schwede et al., 2005). Sea-salt emission is parameterized within CMAQ
166 v5.0.2. While the deposition velocities are calculated inline, the fertilizer ammonia
167 bi-directional flux for in-line emissions and deposition velocities is turned off. Detailed
168 configurations of photolysis, gas-phase chemistry, aqueous chemistry, and aerosol
169 chemistry for CMAQ v5.0.2 are listed in Table 1.

170 2.2 Datasets and evaluation protocols

171 Comprehensive evaluation of the GFSv15-CMAQv5.0.2 forecasting system is
172 conducted for both meteorological and chemical variables for year 2019, including
173 discrete, categorical, and region-specific evaluations. The products in the first 24-hour of
174 each 72-hour forecast cycle are extracted and combined as a continuous, annual forecast.
175 The evaluation of meteorological variables is carried out for those results from PREMAQ
176 in GFSv15-CMAQv5.0.2 system. Detailed information for datasets used in this study is
177 listed in Table S1. Observed hourly temperature at 2-meters (T2), relative humidity at
178 2-meters (RH2), precipitation (Precip), wind direction at 10-meters (WD10), and wind
179 speed at 10-meters (WS10) are obtained from the Clean Air Status and Trends Network
180 (CASTNET) and the METeoro logical Aerodrome Reports (METAR) datasets. The



181 majority of CASTNET sites are suburban and rural sites. Approximately 1900 METAR
182 sites over CONUS are used in this study (Fig. S1). For evaluation of precipitation, a
183 threshold of ≥ 0.1 mm is used for valid records because the CASTNET and METAR have
184 different definitions of 0.0 mm values. In CASTNET, the records without any
185 precipitation are filled as 0.0 mm, the same as those records with negligible precipitation.
186 However, in METAR, the records without any precipitation are left as blank, the same as
187 an invalid record. The negligible precipitation is recorded as 0.0 mm.

188 The air quality forecasting products are evaluated include hourly O_3 , hourly $PM_{2.5}$,
189 maximum daily 8-hour average O_3 (MDA8 O_3), and daily average $PM_{2.5}$ (24-h avg $PM_{2.5}$)
190 for chemical forecast. The AIRNow dataset is used for observed hourly O_3 and $PM_{2.5}$. It
191 is a near real time (NRT) dataset which has preliminary quality control (QC). Many
192 abnormal records are not quality controlled completely. To filter the abnormal records,
193 the thresholds of 120 ppb and $100 \mu\text{g m}^{-3}$ for O_3 and $PM_{2.5}$ are used, respectively. Remote
194 sensing data from the Global Precipitation Climatology Project (GPCP) and the
195 Climatology-Calibrated Precipitation Analysis (CCPA) (Hou et al., 2014; Zhu and Luo,
196 2015) datasets are also used for evaluation of precipitation. GPCP is a global
197 precipitation dataset with a spatial resolution of 0.25 degree and a monthly temporal
198 resolution. The CCPA uses linear regression and downscaling techniques to generate
199 analysis product of precipitation from two datasets: the National Centers for
200 Environmental Prediction (NCEP) CPC Unified Global Daily Gauge Analysis and the



201 NCEP EMC Stage IV multi-sensor quantitative precipitation estimations (QPEs). The
202 CCPA product with a spatial resolution in 0.125 degree and temporal resolution of an
203 hour is used in this study. Satellite-based Aerosol Optical Depth (AOD) at 550 nm from
204 Moderate Resolution Imaging Spectroradiometer (MODIS) Terra platform (Levy et al.,
205 2015) is used for the evaluation of monthly AOD. The statistic measures such as mean
206 bias, the root mean square error (RMSE), the normalized mean bias, the normalized mean
207 error (NME), and the correlation coefficient are used, more details about evaluation
208 protocols are referring to Zhang et al. (2009, 2016). The Taylor diagram (Taylor, 2001),
209 which includes the correlations, NMBs, and the normalized standard deviations (NSD), is
210 used to present the overall performance (Wang et al., 2015). The NMBs $\leq 15\%$ and
211 NMEs $\leq 30\%$ by Zhang et al. (2006) and NMBs ($\leq 15\%$ and $\leq 30\%$), NMEs ($\leq 25\%$ and
212 $\leq 50\%$), and Corr (>0.5 and >0.4) for MDA8 O₃ and 24-h PM_{2.5}, respectively, by Emery
213 et al. (2017) are considered as performance criteria. Monthly, seasonal, and annual
214 statistics and analysis are included. Seasonal analysis for O₃ is separated into ozone
215 season (May-September) and non-ozone season (January-April and October-December).
216 Analysis for ten CONUS regions, defined by U.S. EPA (www.epa.gov/aboutepa), are
217 included and listed in Fig. S1c..

218

219 3. Evaluation of model forecast skills

220 3.1 Evaluation of meteorological forecasts



221 Discrete performance evaluation is conducted for post-processed meteorological
222 fields from the GFSv15-CMAQv5.0.2 system (Table 2). The GFS v15 can predict well
223 the boundary layer meteorological variables. It has overall cold biases and wet biases for
224 annual T2 and RH2 in 2019, respectively. It also overpredicts WS10, and underpredicts
225 hourly precipitation. Despite CASTNET siting being slightly different from that of
226 METAR, the annual and most of the seasonal performance for the model show similar
227 pattern in terms of bias for both the CASTNET and METAR networks. Mean biases of
228 T2 are mostly within ± 0.5 degree Celsius except those in February and March against
229 CASTNET (Table S2). Underprediction is generally larger against CASTNET than
230 METAR. For spatial distribution of MB for seasonal T2 against METAR (Fig. 1), cold
231 biases are mainly found in the Midwest and West U.S. where most of the CASTNET sites
232 are located. GFS v15 usually underpredicts T2 in West Coast, the Mountain States, and
233 the Midwest. Overpredictions of T2 in the states of Kansas, Oklahoma, the areas near the
234 East Coast, and the Gulf Coast offset some underpredictions, resulting in smaller mean
235 biases but similar RMSE for the model against METAR compared to that against
236 CASTNET. The difference between observed T2 from the two datasets is larger in cooler
237 months than warmer months. The largest underpredictions occur in the spring (MAM)
238 season. In general, GFS v15 underpredicts T2 for both CASTNET and METAR,
239 consistent with cold biases found in other studies using GFS v15 (e.g., Yang, 2019). Such
240 underpredictions will affect chemical forecasts, especially the forecast of O₃. Consistent



241 with the overall underpredictions of T2, GFS v15 overpredicts RH2 in general. The
242 largest overprediction is found in spring (MBs of 3.4% and 2.7% with CASTNET and
243 METAR, respectively), corresponding to the largest underprediction of T2 in spring
244 (MBs of -0.5 °C and -0.4 °C with CASTNET and METAR, respectively). GFS v15
245 shows moderately good performance predicting wind. The annual MB and NMB of
246 WS10 against METAR are 0.4 m s⁻¹ and 10.7 %, respectively. A larger overprediction of
247 WS10 is found with CASTNET than other datasets (Zhang et al., 2016).
248 GFSv15-CMAQv5.0.2 also gives higher overpredictions for CASTNET compared to
249 METAR. The largest biases in wind speed are found in summer. GFSv15-CMAQv5.0.2
250 gives the largest cold biases, wet biases in spring, indicating the necessity of improving
251 model performance in such seasons in future GFS-FV3 development.

252 By adopting the threshold of ≥ 0.1 mm, performance against the CASTNET and
253 METAR show similar results: a large underprediction in hourly precipitation. Predicted
254 monthly accumulated precipitation (Fig. S2) shows consistency in spatial distribution
255 with observations from CCPA (Fig. S3) and GPCP (Fig. S4). The high precipitation in
256 the Southeast are captured well in spring while the high precipitation in the Midwest and
257 South are captured well in other seasons. It indicates that GFSv15-CMAQv5.0.2 has good
258 performance in capturing the spatial distributions of accumulated precipitation but has
259 poor performance in predicting hourly precipitation. In the current version of the
260 experimental GFSv15-CMAQv5.0.2 system, the precipitation from original GFS v15



261 output is artificially spread out over time during the preprocessing by the interface
262 preprocessor due to the interpolation using a temporal allocation algorithm. Short rains
263 are interpolated into adjacent time steps (Fig. S5). Such an algorithm leads the model and
264 measurements being more consistent for monthly accumulated precipitation than for
265 discrete hourly precipitation from GFS v15 (which will be resolved by NOAA in the next
266 version of NAQFC based on the GFSv16-CMAQ forecasting system).

267 An overall comparison of performance with CASTNET and METAR datasets is
268 performed using a Taylor diagram (Fig. 2). The normalized standardized deviations
269 (NSDs), Corrs, and NMBs are considered. The NSDs are ratios of variance of predicted
270 values to variance of observed values, following the equations by Wang et al. (2015). The
271 NSDs represent the amplitude of variability. With the NSDs closer to 1, the predicted
272 values have closer variance as the observed values. Consistent with other analysis in this
273 section, larger biases and lower correlation in model wind speed and wind direction are
274 found for CASTNET compared to METAR. The amplitude of variability of WS10
275 against CASTNET is overpredicted (with the NSD larger than 1), while it is
276 underpredicted against METAR. Because of the post-processing smearing of hourly
277 precipitation, the variance of predicted precipitation is smaller than the observed one,
278 leading to very small NSDs for precipitation. The location of the T2 and RH2 points near
279 the REF marker in the Taylor diagram indicates that the GFSv15-CMAQv5.0.2 is
280 capturing the magnitude and variability of these variables well.



281

282 3.2 Evaluation of chemical forecast over the CONUS

283 Performance of chemical forecasts (i.e. O_3 and $PM_{2.5}$) are evaluated on monthly,
284 seasonal, and annual timescales for the studied period of 2019. Performance of the
285 MDA8 O_3 and the 24-h average $PM_{2.5}$ (24-h avg $PM_{2.5}$) are considered as the primary
286 objectives. Categorical performance evaluations for MDA8 O_3 and 24-h avg $PM_{2.5}$ are
287 also conducted. Table 3 shows the discrete statistics of predicted MDA8 O_3 and 24-h avg
288 $PM_{2.5}$ against AIRNow.

289 The GFSv15-CMAQv5.0.2 has good performance for MDA8 O_3 on a seasonal
290 and annual basis with MBs $\leq \pm 1$ ppb, NMB ≤ 2.5 %, and NME ≤ 20 %. The monthly
291 NMBs/NMEs are within ± 15 %/25 %, respectively. Moderate overpredictions and
292 underpredictions are found in both seasons with MB of 0.9 and -0.9 ppb, respectively.
293 The largest underprediction is found in spring months, especially in March.
294 Underprediction of MDA8 O_3 in spring months is consistent with the largest
295 underprediction of T2 in spring. The ozone temperature relationship was found and
296 studied by previous researches (S. Sillman and Samson, 1995; Sillman, 1999). O_3 is
297 expected to increase with increasing temperature within specific range of temperature
298 (Bloomer et al., 2009; Shen et al., 2016). It indicates biases in predicted T2 could be one
299 of the reasons for the corresponding biases in O_3 prediction. Predicted MDA8 O_3 is lower
300 than observed values in major parts of the Midwest and West regions during the O_3



301 season (Fig. 3 and S7), which is consistent with underprediction of T2 in summer. But
302 GFSv15-CMAQv5.0.2 gives very high O₃ in the southeastern U.S., especially in areas
303 near the Gulf Coast. Such overpredictions compensate for moderate underpredictions in
304 Midwest and West, causing an overall overprediction in overall CONUS. Prediction and
305 simulation of O₃ in coastal or marine areas are impacted by halogens chemistry and
306 emissions (Adams and Cox, 2002; Sarwar et al., 2012; Liu et al., 2018), including
307 bromine and iodine chemistry (Foster et al., 2001; Sarwar et al., 2015; Yang et al., 2020)
308 and oceanic halogen emissions (Watanabe, 2005; Tegtmeier et al., 2015; He et al., 2016).
309 CMAQ v5.0.2 has only simple chlorine chemistry for CB05 mechanisms, and the
310 reduction of O₃ by reaction with bromine and iodine is not included in CMAQ v5.0.2.
311 Iodide-mediated O₃ deposition over seawater and detailed marine halogen chemistry has
312 been found to reduce O₃ by 1-4 ppb near the coast (Gantt et al., 2017), suggesting the
313 missing halogen chemistry and O₃ deposition processes contribute to overpredicted O₃ in
314 coastal and marine areas seen here. Coastal and marine areas are also impacted by air-sea
315 interaction processes, which are simply represented in the current meteorological models
316 without coupling oceanic models (He et al., 2018; Zhang et al., 2019c,d). For example,
317 coastal O₃ mixing ratios are impacted by predicted sea surface temperatures and land-sea
318 breezes through their influence on chemical reaction conditions and diffusion processes.
319 As discussed in Section 3.1, T2 is significantly overestimated near the Gulf Coast during
320 summer, which could contribute to biases in O₃ predictions directly or indicate missing



321 land-sea breezes and thus missing transport effects in the GFSv15-CMAQv5.0.2 air
322 quality forecasting system. In the non-O₃ season, GFSv15-CMAQv5.0.2 can forecast
323 well the spatial variations of MDA8 O₃ with overall underpredictions in the Northeast.

324 Unlike the good performance for O₃, GFSv15-CMAQv5.0.2 gives significant
325 overpredictions for 24-h avg PM_{2.5} with annual MB, NMB, and NME of 2.2 μg m⁻³,
326 29.0%, and 65.3%, respectively (Table 3). The MBs and NMBs range from -0.2 μg m⁻³ to
327 5.0 μg m⁻³, and -2.6 % to 59.7 % across the four seasons. With the exception of
328 California and the Southeast, predicted 24-h avg PM_{2.5} shows overprediction during most
329 of the year in spring, autumn, and winter (Fig. 4). Using the historical emission
330 inventories from NEI 2011 and NEI 2014 instead of the latest version of NEI 2017 is one
331 of the reasons for the overpredictions of PM_{2.5} concentrations in 2019. Moderate
332 underpredictions of PM_{2.5} are found in California in spring, autumn, and summer.
333 Murphy et al. (2017) found that secondary organic aerosols (SOA) generated from
334 anthropogenic combustion emissions were important missing PM sources in California
335 prior to CMAQ v5.2. Higher predicted PM_{2.5}, typically SOA, in California is expected in
336 the future using GFS-FV3-CMAQv5.3. The largest underpredictions of PM_{2.5} occur in
337 the Southeast in summer. Biogenic volatile organic compounds (BVOCs) and biogenic
338 SOA (BSOA) are most active in Southeast region in summer. Many missing sources and
339 mechanisms for SOA formation from BVOCs have been identified in recent years (Pye et
340 al., 2013, 2015, 2017; Xu et al., 2018) and have resulted in significant improvements in



341 predicting SOA in the Southeast using CMAQ v5.1 through v5.3. Anthropogenic
342 emissions and aerosol inorganic compounds were found to have impacts on BSOA
343 (Carlton et al., 2018; Pye et al., 2018, 2019). Such interactions and mechanisms are not
344 represented sufficiently in CMAQ v5.0.2, further enhancing the biases in predicted $PM_{2.5}$
345 in the Southeast. In general, updating NAQFC with CMAQ v5.3 is expected to reduce the
346 biases in California and the Southeast.

347 Categorical evaluation is conducted to quantify the accuracy of the
348 GFSv15-CMAQv5.0.2 system in predicting events in which the air pollutants exceed
349 moderate or unhealthy categories for the U.S. air quality index (AQI) (www.airnow.gov).
350 The metrics of False Alarm Ratio (FAR) and the Hit Rate (H) are used (Kang et al., 2005;
351 Barnes et al., 2009). The scatter plots for predicted and observed MDA8 O_3 and 24-h avg
352 $PM_{2.5}$ are shown in Fig. 5a and Fig. 5b, respectively. The plots are divided into four areas
353 based on whether the predicted and/or observed data fall above or below the AQI
354 thresholds: (a) observed values \leq thresholds and predicted values $>$ thresholds; (b)
355 observed and predicted values $>$ thresholds; (c) observed and predicted values \leq
356 thresholds; (d) observed values $>$ thresholds and predicted values \leq thresholds. The FAR
357 and H are defined in Eq. (1) and Eq. (2):

358
$$FAR = \frac{a}{a+b} \times 100\% \quad (1)$$

359
$$H = \frac{b}{b+d} \times 100\% \quad (2).$$



360 Numbers of the scatters in the four areas (a) to (d) are indicated in the equations. The
361 higher the FAR is, the more GFSv15-CMAQv5.0.2 overpredicts the AQI leading to false
362 air quality warnings. The higher the H is, exceedances are more successfully captured by
363 the GFSv15-CMAQv5.0.2 system. In this study, the thresholds for two categories of
364 “Moderate” and “Unhealthy for Sensitive Groups” are considered. Since 2018, they are
365 defined as 55 ppb and 70 ppb for MDA8 O₃ and 12 μg m⁻³ and 35.5 μg m⁻³ for 24-h avg
366 PM_{2.5}. For comparison with previous studies, the historical thresholds are also included
367 into the evaluation: 60 ppb and 75 ppb for MDA8 O₃ and 15 μg m⁻³ and 35 μg m⁻³ for
368 24-h avg PM_{2.5}. The metrics in four categories, corresponding to four thresholds, are
369 shown in Fig. 5c. Categorical performance under stricter AQI standards is better than
370 under historical standards. For example, the FAR decreases from 47.8 % to 41.1 %, and
371 the H increases from 40.3 % to 43.9 % with the “Moderate” thresholds change from 60
372 ppb to 55 ppb. It could be due to the better performance of the forecast system for values
373 closer to the annual average level (~40 ppb). The scatters are more discrete for extreme
374 values (Fig. 5a). When the thresholds of MDA8 O₃ are closer to the average level, the
375 categorical performance increases. The categorical performance of
376 GFSv15-CMAQv5.0.2 in predicting MDA8 O₃ is close to the performance of the
377 previous NAQFC (Kang et al., 2010). Similar improvement in the FAR and H for
378 predicting categorical 24-h avg PM_{2.5} can be found when the threshold changes from 15
379 μg m⁻³ to 12 μg m⁻³: the FAR decreases from 79.7 % to 70.1 %, and the H increases from



380 51.9 % to 57.0 %. However, the FAR is high (over 90%) and the H is much lower under
381 the threshold of $35.5 \mu\text{g m}^{-3}$. It is because most of the false alarms occur when observed
382 24-h avg $\text{PM}_{2.5}$ are lower than $20 \mu\text{g m}^{-3}$ and the predicted values are higher than $20 \mu\text{g}$
383 m^{-3} (Fig. 5b). It shows the poorer performance in correctly capturing the category of
384 “Unhealthy for Sensitive Groups” due to the significant overprediction of $\text{PM}_{2.5}$ in cooler
385 months.

386 Evaluation of predicted AOD against observations from MODIS is shown in Fig.
387 6. High predicted AOD in the Midwest during cooler months show consistency with
388 MODIS and correspond to high surface $\text{PM}_{2.5}$ predictions. High predicted AOD are
389 missing in California, corresponding to underprediction of surface $\text{PM}_{2.5}$ in California. In
390 summer months, AOD is largely underpredicted in California and the Southeast region,
391 which may be caused by the previously mentioned missing sources of SOA.

392 To further analyze the major source for spatial and temporal biases in predicted
393 $\text{PM}_{2.5}$, key chemical components of $\text{PM}_{2.5}$ in January, July, and August are depicted in
394 Fig. 7. Extremely high particulate sulfate and organic carbon, generated by large wildfires,
395 are carried in from the north boundary in July. The forecast spatial pattern agrees well
396 with the observed AOD in July. High concentrations of $\text{PM}_{2.5}$ associated with soil
397 components, unspecified coarse mode components, and high particulate NO_3^-
398 concentrations are major contributors to the high $\text{PM}_{2.5}$ in the Midwest. The soil
399 components are estimated using the Interagency Monitoring of Protected Visual



400 Environments (IMPROVE) equation and specific constituents (Appel et al., 2013). These
401 high concentrations are caused by large emissions of anthropogenic primary PM_{2.5},
402 primary coarse PM, ammonia (NH₃), and NO_x in the Midwest (Fig. S6). The large
403 emissions of anthropogenic primary coarse PM, as well as the wind-blown dust are the
404 major sources for soil components and unspecified coarse mode components. Appel et al.
405 (2013) also indicated CMAQ overpredicts soil components, sources of which include
406 fugitive and wind-blown dust, in the eastern United States.

407

408 3.3 Region-specific evaluation

409 As discussed in section 3.2, biases in predicted O₃ and PM_{2.5} vary from region to
410 region. To further analyze the region-specific performance of the GFSv15-CMAQv5.0.2
411 system, evaluation for 10 regions within CONUS is conducted. By identifying the
412 detailed characteristics of region-specific biases and indicating the underlying causes for
413 such biases, this section aims to help the NAQFC to improve its forecast ability for
414 specific regions. A science-based bias correction method will be developed for the
415 operational GFS-FV3-CMAQ system in the future. This section can also contribute to
416 hypotheses that may serve as a scientific basis for future bias correction methods.

417 Figure 8 shows the annual model performance for MDA8 O₃ and 24-h avg PM_{2.5}
418 in the 10 CONUS regions. In section 3.2, a slight underprediction of MDA8 O₃ on annual



419 basis was found over the CONUS. MDA8 O₃ is overpredicted in most of the regions
420 except regions 2, 4, and 6 (Fig. 8a). The overpredictions in regions 4 and 6 are mostly
421 from the large biases near the coast area during O₃ season. Correlations between
422 predictions and observations in most of the regions are higher than 0.6, except for 0.55 in
423 region 4 and 0.50 in region 7. Poor performance in regions 4 and 7 is illustrated by the
424 Taylor Diagram (Fig. 8b). Small Corr and NSD, result in the markers of regions 4 and 7
425 laying farthest from the reference point. The amplitude of variability of the predicted
426 MDA8 O₃ are smaller than observed values in all the regions, especially in regions 4 and
427 7. The performance in region 2 is the best, with smallest MB/NMB, highest Corr, and
428 similar variability in predictions and observations. The time series of the MDA8 O₃ for
429 the 10 regions during 2019 is shown in Fig. S7. Regions 1, 2, 4, and 6 show different
430 results for the O₃ season and non-O₃ season: GFSv15-CMAQv5.0.2 tends to overpredict
431 MDA8 O₃ during the O₃ season and underpredicts during the non-O₃ season. The
432 underprediction during spring months, which is indicated in section 3.2, can be also
433 found in most of the regions with obvious gaps between observed and predicted curves in
434 March and April. The lowest O₃ predictions occur at 5 am local standard time (LST) in
435 most of the regions (Fig. S8). For regions 4 and 6, significant overprediction occurs not
436 only during the O₃ season for MDA8 O₃ (which mainly occurs during the daytime) but
437 also during the nighttime. During the non-O₃ season, the biases in predicting MDA8 O₃
438 for regions 4 and 6 are small and consistent with good daytime predictions. However, O₃



439 is still overpredicted during the nighttime in these regions, associated with the collapse of
440 the boundary layer and difficulty in simulating its time and magnitude (Hu et al., 2013;
441 Cuchiara et al., 2014; Pleim et al., 2016).

442 Consistent with the analysis in section 3.2, $PM_{2.5}$ is significantly overpredicted in
443 most of the regions except in regions 4, 6, and 9 (Fig. 8c). The underprediction during
444 warmer months, likely due to missing sources and mechanisms for BSOA, compensate
445 for the annual biases in regions 4 and 6, leading to smaller MBs/NMBs but low
446 correlations in these regions. The variability in predictions is much larger than in
447 observations, with the NSDs >1 for all regions (Fig. 8d). The forecast system has best
448 performance in region 9 with an NSD of 1.2, an NMB of -12.0 %, and a Corr of 0.40. As
449 discussed in section 3.2, the performance of predicted $PM_{2.5}$ in region 9 is expected to be
450 further improved with the updates in CMAQ v5.3, specifically the representation of
451 anthropogenic SOA.

452 Figure S9 shows the time series of 24-h avg $PM_{2.5}$ in the 10 CONUS regions. The
453 gaps between observed and predicted curves are large in cooler months, but the
454 GFSv15-CMAQv5.0.2 system has relatively good performance in warmer months for
455 most of the regions. Less overprediction is found in regions 6, 8, and 9 during cooler
456 months, and those regions generally show the best performance (see Taylor Diagram).
457 The different biases across the regions further indicate that multiple factors likely
458 contribute to them. To further analyze the underlying causes for varied patterns and



459 performance on season- and region-specific basis, diurnal evaluations for $PM_{2.5}$ and
460 chemical components of $PM_{2.5}$ during O_3 season and non- O_3 season are shown in Fig. 9.
461 The GFSv15-CMAQv5.0.2 has a large seasonal variation in diurnal $PM_{2.5}$, inconsistent
462 with the observation. While $PM_{2.5}$ is underpredicted during daytime in regions 4, 6, 8,
463 and 9 during O_3 season, $PM_{2.5}$ is always overpredicted across the day during non- O_3
464 season except for region 9. Increased OC, particulate nitrates, soil and unspecified coarse
465 mode components contribute to most of the increase in predicted total $PM_{2.5}$. The general
466 cold biases over CONUS, especially in region 5, could make the GFSv15-CMAQv5.0.2
467 system predict higher nitrate particulates, leading to larger increase in $PM_{2.5}$ from O_3
468 season to non- O_3 season. Emissions vary from month to month in the year (Fig. S10).
469 Larger emissions for NH_3 , NO_x , VOC, primary coarse PM, and primary $PM_{2.5}$ are in O_3
470 season compared to non- O_3 season. Primary organic carbons (POC) emissions are higher
471 in O_3 season. Changes in emissions are not fully consistent with the changes in $PM_{2.5}$
472 components, indicating other biases or uncertainty could also contribute to the significant
473 overprediction during non- O_3 season. For example, the implementation of bidirectional
474 flux of NH_3 and the boundary layer mixing processes under more stable condition (during
475 non- O_3 season) in GFSv15-CMAQv5.0.2 system need to be further studied. Pleim et al.,
476 (2013, 2019) found that the NH_3 fluxes and concentrations could be better simulated and
477 the monthly variations of NH_3 concentrations were larger comparing to the raw model by
478 implementing the bidirectional flux of NH_3 . The absolute biases for diurnal $PM_{2.5}$ are



479 generally larger during nighttime in most of the regions, except for region 9. It is
480 consistent with the analysis by Appel et al. (2013), which suggested that the efforts of
481 improving nighttime mixing in CMAQ v5.0 be further needed, further indicating the need
482 for improvements of CMAQ in predicting dispersion and mixing of air pollutants under
483 stable boundary layer conditions.

484

485 **4. Conclusion**

486 In this work, the air quality forecast for the year 2019 predicted by the
487 offline-coupled GFSv15-CMAQv5.0.2 system is comprehensively evaluated. The
488 GFSv15-CMAQv5.0.2 system is found to perform well in predicting surface
489 meteorological variables (temperature, relative humidity, and wind) and O₃ but has mixed
490 performance for PM_{2.5}. Moderate cold biases and wet biases are found in spring season,
491 especially in March. While the GFSv15-CMAQv5.0.2 system can generally capture the
492 monthly accumulated precipitation compared to remote sensing and ensemble datasets,
493 temporal distributions of hourly precipitation show less consistency with in-situ
494 monitoring data, which is attributed to the interpolation and post-processing in the
495 offline-coupling interface preprocessor.

496 MDA8 O₃ is slightly overpredicted and underpredicted in ozone and non-ozone
497 seasons, respectively. The cold biases of T2 contribute to the underprediction of MDA8



498 O₃ in spring. The significant overprediction near the Gulf Coast, which is caused by
499 missing halogen chemistry and the missing of model representation of the air-sea
500 interaction processes, compensates for underprediction in the West and Midwest in O₃
501 season for nation-wide metrics. GFSv15-CMAQv5.0.2 has poorer performance in
502 predicting PM_{2.5}, comparing to the performance for O₃. Significant overpredictions are
503 found in spring, autumn, and winter, with the largest overprediction in the Midwest, WA,
504 and Oregon, due mainly to high concentrations of predicted soil, unspecified coarse mode
505 and nitrate components. The overall cold biases in the Region 5/Midwest could contribute
506 to higher predicted nitrate particulate matter but overprediction of PM_{2.5} in the region is
507 likely driven by sources containing trace metals such as anthropogenic fugitive dust and
508 wind-blown dust. The forecasting system may be improved through updating the
509 emissions inventory used (i.e., NEI 2014) to NEI 2016v2 or NEI 2017 which are more
510 presentative to the year of 2019 in the next development of next-generation NAQFC.

511 Categorical evaluation indicates that the GFSv15-CMAQv5.0.2 can capture well
512 the air quality classification of “Moderate” described by the AQI. However, the
513 categorical performance is poorer for PM_{2.5} at the “unhealthy for sensitive groups”
514 threshold due mainly to the significant overprediction during the cooler months.
515 Region-specific evaluation further discusses the biases and underlying causes in the 10
516 USEPA defined regions in CONUS. An update from CMAQ v5.0.2 to v5.3.1 is expected
517 to alleviate potential errors in missing sources and mechanisms for SOA formation. The



518 variations of performance in between O₃ and non-O₃ seasons, as well as during the
519 daytime and nighttime, indicate further studies need to be conducted to improve boundary
520 layer mixing processes within GFSv15-CMAQv5.0.2. The varied region-specific
521 performance indicates that improvements, such as bias corrections, should be considered
522 individually from region to region in the following development of the next generation
523 NAQFC.

524 We have used bias analyses in this work to identify several areas of weakness for
525 further improvement and development of next-generation NAQFC. Further studies are
526 still needed for improving the emissions, the aerosol chemistry, and the boundary layer
527 mixing for the future GFS-FV3-CMAQ system. Our work and the further studies can
528 provide information and scientific basis for the development and implement of a
529 science-based bias correction method in next-generation NAQFC.

530

531 **Supplement**

532 The supplement related to this article is available in
533 [gmd-2020-272_supplement.pdf](#)

534

535 **Code and data availability**



536 The documentation and source code of CMAQ v5.0.2 are available at
537 doi:10.5281/zenodo.1079898. The GFS forecasts in grib2 format are available at
538 <https://www.ncdc.noaa.gov/data-access/model-data/model-datasets/global-forecast-system>
539 -gfs. The GFS forecast inputs in binary (nemsio) format and the coupler used in this study
540 for the GFSv15-CMAQv5.0.2 system are available upon request. The AIRNow data is
541 available for download through the AirNow-Tech website (<http://www.airnowtech.org>).
542 The CASTNET data is available for download from
543 <https://java.epa.gov/castnet/clearsession.do>. The METAR data is available for download
544 from <https://madis.ncep.noaa.gov>. The GPCP data is available through NOAA website
545 (<https://www.ncei.noaa.gov/data/global-precipitation-climatology-project-gpcp-monthly>).
546 The CCPA precipitation is available from
547 <https://www.nco.ncep.noaa.gov/pmb/products/gens>. The MODIS_MOD04 dataset is
548 available at dx.doi.org/10.5067/MODIS/MOD04_L2.006. The data processing and
549 analysis scripts are available upon request.

550

551 **Author contribution**

552 YZ and DT defined the scope and focus of the manuscript and designed the model
553 simulations. XC and YZ developed the paper outline and structure. PL, JH, YT, and JM
554 performed the forecast simulations. YT generated the emissions and PC generated the
555 lateral boundary conditions for the model simulations. XC performed the model



556 evaluation and drafted the manuscript. XC and KW developed postprocessing and
557 statistical scripts. HP, BM, and DK assisted in analysis of region-specific biases. YZ, HP,
558 DK, BM, JH, PC, PL, DT, and KW reviewed the manuscript.

559

560 **Competing interests**

561 The authors declare that they have no conflict of interest.

562

563 **Acknowledgements**

564 This project is sponsored by NOAA Office of Weather and Air Quality through
565 grant #NA19OAR4590084 at North Carolina State University, #NA20OAR4590259 at
566 Northeastern University and #NA19OAR4590085 at George Mason University. Thanks
567 to Fanglin Yang for providing information regarding GFS v15. High performance
568 computing at Northeastern University was support by the Stampede XSEDE high
569 performance computing support under the NSF ACI 1053575.

570

571 **Disclaimer**

572 The scientific results and conclusions, as well as any views or opinions expressed
573 herein, are those of the author(s) and do not necessarily reflect the views of NOAA or the



574 Department of Commerce. The views expressed in this document are solely those of the
575 authors and do not necessarily reflect those of the U.S. EPA. EPA does not endorse any
576 products or commercial services mentioned in this publication.

577

578 **References**

- 579 Adams, J. W. and Cox, R. A.: Halogen chemistry of the marine boundary layer, *J. Phys.*
580 *IV*, 12(10), 105–124, doi:10.1051/jp4:20020455, 2002.
- 581 Appel, K. W., Pouliot, G. A., Simon, H., Sarwar, G., Pye, H. O. T., Napelenok, S. L.,
582 Akhtar, F. and Roselle, S. J.: Evaluation of dust and trace metal estimates from the
583 Community Multiscale Air Quality (CMAQ) model version 5.0, *Geosci. Model Dev.*,
584 6(4), 883–899, doi:10.5194/gmd-6-883-2013, 2013.
- 585 Arakawa, A. and Lamb, V. R.: Computational design of the basic dynamical processes of
586 the UCLA general circulation model, 1977.
- 587 Arakawa, A. and Schubert, W. H.: Interaction of a Cumulus Cloud Ensemble with the
588 Large-Scale Environment, Part I, *J. Atmos. Sci.*, 31(3), 674–701,
589 doi:10.1175/1520-0469(1974)031<0674:IOACCE>2.0.CO;2, 1974.
- 590 Barnes, L. R., Schultz, D. M., Gruntfest, E. C., Hayden, M. H. and Benight, C. C.:
591 Corrigendum: False alarm rate or false alarm ratio?, *Weather Forecast.*, 24(5),
592 1452–1454, doi:10.1175/2009WAF2222300.1, 2009.



- 593 Binkowski, F. S., Arunachalam, S., Adelman, Z. and Pinto, J. P.: Examining photolysis
594 rates with a prototype online photolysis module in CMAQ, *J. Appl. Meteorol.*
595 *Climatol.*, 46(8), 1252–1256, doi:10.1175/JAM2531.1, 2007.
- 596 Black, T. L.: The New NMC Mesoscale Eta Model: Description and Forecast Examples,
597 *Weather Forecast.*, 9(2), 265–278,
598 doi:10.1175/1520-0434(1994)009<0265:TNNMEM>2.0.CO;2, 1994.
- 599 Bloomer, B. J., Stehr, J. W., Piety, C. A., Salawitch, R. J. and Dickerson, R. R.: Observed
600 relationships of ozone air pollution with temperature and emissions, *Geophys. Res.*
601 *Lett.*, 36(9), doi:10.1029/2009GL037308, 2009.
- 602 Byun, D. and Schere, K. L.: Review of the governing equations, computational
603 algorithms, and other components of the models-3 community multiscale air quality
604 (CMAQ) modeling system, *Appl. Mech. Rev.*, 59(1–6), 51–77,
605 doi:10.1115/1.2128636, 2006.
- 606 Carlton, A. G., Bhave, P. V., Napelenok, S. L., Edney, E. O., Sarwar, G., Pinder, R. W.,
607 Pouliot, G. A. and Houyoux, M.: Model representation of secondary organic aerosol
608 in CMAQv4.7, *Environ. Sci. Technol.*, 44(22), 8553–8560, doi:10.1021/es100636q,
609 2010.
- 610 Carlton, A. G., Pye, H. O. T., Baker, K. R. and Hennigan, C. J.: Additional Benefits of
611 Federal Air-Quality Rules: Model Estimates of Controllable Biogenic Secondary



- 612 Organic Aerosol, Environ. Sci. Technol., 52(16), 9254–9265,
613 doi:10.1021/acs.est.8b01869, 2018.
- 614 Chen, F., Janjić, Z. and Mitchell, K.: Impact of atmospheric surface-layer
615 parameterizations in the new land-surface scheme of the NCEP mesoscale Eta model,
616 Boundary-Layer Meteorol., 85(3), 391–421, doi:10.1023/A:1000531001463, 1997.
- 617 Chuang, M. T., Zhang, Y. and Kang, D.: Application of WRF/Chem-MADRID for
618 real-time air quality forecasting over the Southeastern United States, Atmos.
619 Environ., 45(34), 6241–6250, doi:10.1016/j.atmosenv.2011.06.071, 2011.
- 620 Clough, S. A., Shephard, M. W., Mlawer, E. J., Delamere, J. S., Iacono, M. J.,
621 Cady-Pereira, K., Boukabara, S. and Brown, P. D.: Atmospheric radiative transfer
622 modeling: A summary of the AER codes, J. Quant. Spectrosc. Radiat. Transf., 91(2),
623 233–244, doi:10.1016/j.jqsrt.2004.05.058, 2005.
- 624 Cuchiara, G. C., Li, X., Carvalho, J. and Rappenglück, B.: Intercomparison of planetary
625 boundary layer parameterization and its impacts on surface ozone concentration in
626 the WRF/Chem model for a case study in houston/texas, Atmos. Environ., 96,
627 175–185, doi:10.1016/j.atmosenv.2014.07.013, 2014.
- 628 Eder, B., Kang, D., Mathur, R., Yu, S. and Schere, K.: An operational evaluation of the
629 Eta-CMAQ air quality forecast model, Atmos. Environ., 40(26), 4894–4905,
630 doi:10.1016/j.atmosenv.2005.12.062, 2006.



- 631 Eder, B., Kang, D., Mathur, R., Pleim, J., Yu, S., Otte, T. and Pouliot, G.: A performance
632 evaluation of the National Air Quality Forecast Capability for the summer of 2007,
633 Atmos. Environ., 43(14), 2312–2320, doi:10.1016/j.atmosenv.2009.01.033, 2009.
- 634 Emery, C., Jung, J., Koo, B., Yarwood, G.: Improvements to CAMx Snow Cover
635 Treatments and Carbon Bond Chemical Mechanism for Winter Ozone. Final report
636 for Utah DAQ, project UDAQ PO 480 52000000001, 2015.
- 637 Emery, C., Liu, Z., Russell, A. G., Odman, M. T., Yarwood, G. and Kumar, N.:
638 Recommendations on statistics and benchmarks to assess photochemical model
639 performance, J. Air Waste Manag. Assoc., 67(5), 582–598,
640 doi:10.1080/10962247.2016.1265027, 2017.
- 641 Foster, K. L., Plastridge, R. A., Bottenheim, J. W., Shepson, P. B., Finlayson-Pitts, B. J.
642 and Spicer, C. W.: The role of Br₂ and BrCl in surface ozone destruction at polar
643 sunrise, Science (80-.), 291(5503), 471–474, doi:10.1126/science.291.5503.471,
644 2001.
- 645 Gantt, B., Sarwar, G., Xing, J., Simon, H., Schwede, D., Hutzell, W. T., Mathur, R. and
646 Saiz-Lopez, A.: The Impact of Iodide-Mediated Ozone Deposition and Halogen
647 Chemistry on Surface Ozone Concentrations Across the Continental United States,
648 Environ. Sci. Technol., 51(3), 1458–1466, doi:10.1021/acs.est.6b03556, 2017.
- 649 Grell, G. A.: Prognostic Evaluation of Assumptions Used by Cumulus Parameterizations,



- 650 Mon. Weather Rev., 121(3), 764–787,
651 doi:10.1175/1520-0493(1993)121<0764:PEOAUB>2.0.CO;2, 1993.
- 652 He, J., He, R. and Zhang, Y.: Impacts of Air-sea Interactions on Regional Air Quality
653 Predictions Using a Coupled Atmosphere-ocean Model in Southeastern U.S.,
654 Aerosol Air Qual. Res., 18(4), 1044–1067, doi:10.4209/aaqr.2016.12.0570, 2018.
- 655 He, P., Bian, L., Zheng, X., Yu, J., Sun, C., Ye, P. and Xie, Z.: Observation of surface
656 ozone in the marine boundary layer along a cruise through the Arctic Ocean: From
657 offshore to remote, Atmos. Res., 169, 191–198, doi:10.1016/j.atmosres.2015.10.009,
658 2016.
- 659 Hou, D., Charles, M., Luo, Y., Toth, Z., Zhu, Y., Krzysztofowicz, R., Lin, Y., Xie, P.,
660 Seo, D. J., Pena, M. and Cui, B.: Climatology-calibrated precipitation analysis at fine
661 scales: Statistical adjustment of stage IV toward CPC gauge-based analysis, J.
662 Hydrometeorol., 15(6), 2542–2557, doi:10.1175/JHM-D-11-0140.1, 2014.
- 663 Hu, X. M., Klein, P. M. and Xue, M.: Evaluation of the updated YSU planetary boundary
664 layer scheme within WRF for wind resource and air quality assessments, J. Geophys.
665 Res. Atmos., 118(18), 10,490-10,505, doi:10.1002/jgrd.50823, 2013.
- 666 Huang, J., McQueen, J., Wilczak, J., Djalalova, I., Stajner, I., Shafran, P., Allured, D.,
667 Lee, P., Pan, L., Tong, D., Huang, H.-C., DiMego, G., Upadhayay, S. and Delle
668 Monache, L.: Improving NOAA NAQFC PM 2.5 Predictions with a Bias Correction



- 669 Approach, *Weather Forecast.*, 32(2), 407–421, doi:10.1175/WAF-D-16-0118.1,
670 2017.
- 671 Huang, J., McQueen, J., Shafran, P., Huang, H., Kain, J., Tang, Y., Lee, P., Stajner, I. and
672 Tirado-Delgado, J.: Development and evaluation of offline coupling of FV3-based
673 GFS with CMAQ at NOAA, the 17th CMAS Conference, UNC-Chapel Hill, NC,
674 22-24 October 2018, 2018.
- 675 Huang, J., McQueen, J., Yang, B., Shafran, P., Pan, L., Huang, H., Bhattacharjee, P.,
676 Tang, Y., Campbell, P., Tong, D., Lee, P., Stajner, I., Kain, J., Tirado-Delgado, J.
677 and Koch, D.: Impact of global scale FV3 versus regional scale NAM meteorological
678 driver model predictions on regional air quality forecasting. The 100th AGU Fall
679 Meeting, San Francisco, CA, 9-13 December 2019, 2019.
- 680 Iacono, M. J., Mlawer, E. J., Clough, S. A. and Morcrette, J.-J.: Impact of an improved
681 longwave radiation model, RRTM, on the energy budget and thermodynamic
682 properties of the NCAR community climate model, CCM3, *J. Geophys. Res. Atmos.*,
683 105(D11), 14873–14890, doi:10.1029/2000JD900091, 2000.
- 684 Kang, D., Eder, B. K., Stein, A. F., Grell, G. A., Peckham, S. E. and Mc Henry, J.: The
685 New England Air Quality Forecasting Pilot Program: Development of an Evaluation
686 Protocol and Performance Benchmark, *J. Air Waste Manag. Assoc.*, 55(12),
687 1782–1796, doi:10.1080/10473289.2005.10464775, 2005.



- 688 Kang, D., Mathur, R., Rao, S. T. and Yu, S.: Bias adjustment techniques for improving
689 ozone air quality forecasts, *J. Geophys. Res.*, 113(D23), D23308,
690 doi:10.1029/2008JD010151, 2008.
- 691 Kang, D., Mathur, R. and Trivikrama Rao, S.: Assessment of bias-adjusted PM_{2.5} air
692 quality forecasts over the continental United States during 2007, *Geosci. Model Dev.*,
693 3(1), 309–320, doi:10.5194/gmd-3-309-2010, 2010a.
- 694 Kang, D., Mathur, R. and Trivikrama Rao, S.: Real-time bias-adjusted O₃ and PM_{2.5} air
695 quality index forecasts and their performance evaluations over the continental United
696 States, *Atmos. Environ.*, 44(18), 2203–2212, doi:10.1016/j.atmosenv.2010.03.017,
697 2010b.
- 698 Lee, P., Ngan, F., Kim, H., Tong, D., Tang, Y., Chai, T., Saylor, R., Stein, A., Byun, D.,
699 Tsidulko, M., McQueen, J. and Stajner, I.: Incremental Development of Air Quality
700 Forecasting System with Off-Line/On-Line Capability: Coupling CMAQ to NCEP
701 National Mesoscale Model, in *Air Pollution Modeling and its Application XXI*, pp.
702 187–192, Springer, Dordrecht., 2011.
- 703 Lee, P., McQueen, J., Stajner, I., Huang, J., Pan, L., Tong, D., Kim, H., Tang, Y.,
704 Kondragunta, S., Ruminski, M., Lu, S., Rogers, E., Saylor, R., Shafran, P., Huang,
705 H.-C., Gorline, J., Upadhyay, S. and Artz, R.: NAQFC Developmental Forecast
706 Guidance for Fine Particulate Matter (PM_{2.5}), *Weather Forecast.*, 32(1), 343–360,



- 707 doi:10.1175/waf-d-15-0163.1, 2017.
- 708 Levy, R. and Hsu, C.: MODIS Atmosphere L2 Aerosol Product. NASA MODIS
709 Adaptive Processing System, Goddard Space Flight Center, USA:
710 http://dx.doi.org/10.5067/MODIS/MOD04_L2.006, 2015.
- 711 Liu, Y., Fan, Q., Chen, X., Zhao, J., Ling, Z., Hong, Y., Li, W., Chen, X., Wang, M. and
712 Wei, X.: Modeling the impact of chlorine emissions from coal combustion and
713 prescribed waste incineration on tropospheric ozone formation in China, *Atmos.*
714 *Chem. Phys.*, 18(4), 2709–2724, doi:10.5194/acp-18-2709-2018, 2018.
- 715 Lu, C.-H., da Silva, A., Wang, J., Moorthi, S., Chin, M., Colarco, P., Tang, Y.,
716 Bhattacharjee, P. S., Chen, S.-P., Chuang, H.-Y., Juang, H.-M. H., McQueen, J. and
717 Iredell, M.: The implementation of NEMS GFS Aerosol Component (NGAC)
718 Version 1.0 for global dust forecasting at NOAA/NCEP, *Geosci. Model Dev.*, 9(5),
719 1905–1919, doi:10.5194/gmd-9-1905-2016, 2016.
- 720 Mathur, R., Yu, S., Kang, D. and Schere, K. L.: Assessment of the wintertime
721 performance of developmental particulate matter forecasts with the Eta-Community
722 Multiscale Air Quality modeling system, *J. Geophys. Res.*, 113(D2), D02303,
723 doi:10.1029/2007JD008580, 2008.
- 724 McHenry, J. N., Ryan, W. F., Seamn, N. L., Coats, C. J., Pudykiewicz, J., Arunachalam,
725 S. and Vukovich, J. M.: A real-time eulerian photochemical model forecast system,



- 726 Bull. Am. Meteorol. Soc., 85(4), 525–548, doi:10.1175/BAMS-85-4-525, 2004.
- 727 McKeen, S., Wilczak, J., Grell, G., Djalalova, I., Peckham, S., Hsie, E.-Y., Gong, W.,
728 Bouchet, V., Menard, S., Moffet, R., McHenry, J., McQueen, J., Tang, Y.,
729 Carmichael, G. R., Pagowski, M., Chan, A., Dye, T., Frost, G., Lee, P. and Mathur,
730 R.: Assessment of an ensemble of seven real-time ozone forecasts over eastern North
731 America during the summer of 2004, *J. Geophys. Res.*, 110(D21), D21307,
732 doi:10.1029/2005JD005858, 2005.
- 733 McKeen, S., Chung, S. H., Wilczak, J., Grell, G., Djalalova, I., Peckham, S., Gong, W.,
734 Bouchet, V., Moffet, R., Tang, Y., Carmichael, G. R., Mathur, R. and Yu, S.:
735 Evaluation of several PM_{2.5} forecast models using data collected during the
736 ICARTT/NEAQS 2004 field study, *J. Geophys. Res. Atmos.*, 112(D10),
737 doi:10.1029/2006JD007608, 2007.
- 738 McKeen, S., Grell, G., Peckham, S., Wilczak, J., Djalalova, I., Hsie, E.-Y., Frost, G.,
739 Peischl, J., Schwarz, J., Spackman, R., Holloway, J., de Gouw, J., Warneke, C.,
740 Gong, W., Bouchet, V., Gaudreault, S., Racine, J., McHenry, J., McQueen, J., Lee, P.,
741 Tang, Y., Carmichael, G. R. and Mathur, R.: An evaluation of real-time air quality
742 forecasts and their urban emissions over eastern Texas during the summer of 2006
743 Second Texas Air Quality Study field study, *J. Geophys. Res.*, 114(12), D00F11,
744 doi:10.1029/2008JD011697, 2009.



- 745 Mlawer, E. J., Taubman, S. J., Brown, P. D., Iacono, M. J. and Clough, S. A.: Radiative
746 transfer for inhomogeneous atmospheres: RRTM, a validated correlated-k model for
747 the longwave, *J. Geophys. Res. D Atmos.*, 102(14), 16663–16682,
748 doi:10.1029/97jd00237, 1997.
- 749 Murphy, B. N., Woody, M. C., Jimenez, J. L., Carlton, A. M. G., Hayes, P. L., Liu, S.,
750 Ng, N. L., Russell, L. M., Setyan, A., Xu, L., Young, J., Zaveri, R. A., Zhang, Q. and
751 Pye, H. O. T.: Semivolatile POA and parameterized total combustion SOA in
752 CMAQv5.2: Impacts on source strength and partitioning, *Atmos. Chem. Phys.*,
753 17(18), 11107–11133, doi:10.5194/acp-17-11107-2017, 2017.
- 754 National Centers for Environmental Prediction: The Global Forecast System (GFS) -
755 Global Spectral Model (GSM). Retrieved from
756 [https://www.emc.ncep.noaa.gov/emc/pages/numerical_forecast_systems/gfs/documentation.](https://www.emc.ncep.noaa.gov/emc/pages/numerical_forecast_systems/gfs/documentation.php)
757 php, last access: May 2020, 2019a.
- 758 National Centers for Environmental Prediction: FV3: The GFDL Finite-Volume
759 Cubed-Sphere Dynamical Core, Retrieved from
760 <https://vlab.ncep.noaa.gov/web/fv3gfs>, last access: May 2020, 2019b.
- 761 Otte, T. L., Pouliot, G., Pleim, J. E., Young, J. O., Schere, K. L., Wong, D. C., Lee, P. C.
762 S., Tsidulko, M., McQueen, J. T., Davidson, P., Mathur, R., Chuang, H.-Y., DiMego,
763 G. and Seaman, N. L.: Linking the Eta Model with the Community Multiscale Air



- 764 Quality (CMAQ) Modeling System to Build a National Air Quality Forecasting
765 System, *Weather Forecast.*, 20(3), 367–384, doi:10.1175/WAF855.1, 2005.
- 766 Patrick, C., Tang, Y., Lee, P., Baker, B., Tong, D., Saylor, R., Huang, J., Huang, H.,
767 McQueen, J. and Stajne, I.: An Improved National Air Quality Forecasting
768 Capability Using the NOAA Global Forecast System Version 16. In preparation,
769 2020.
- 770 Pleim, J., Gilliam, R., Appel, W. and Ran, L.: Recent Advances in Modeling of the
771 Atmospheric Boundary Layer and Land Surface in the Coupled WRF-CMAQ Model
772 BT - Air Pollution Modeling and its Application XXIV, in *Air Pollution Modeling
773 and its Application XXIV*, edited by D. G. Steyn and N. Chaumerliac, pp. 391–396,
774 Springer International Publishing, Cham., 2016.
- 775 Pleim, J. E., Bash, J. O., Walker, J. T. and Cooter, E. J.: Development and evaluation of
776 an ammonia bidirectional flux parameterization for air quality models, *J. Geophys.
777 Res. Atmos.*, 118(9), 3794–3806, doi:10.1002/jgrd.50262, 2013.
- 778 Pleim, J. E., Ran, L., Appel, W., Shephard, M. W. and Cady-Pereira, K.: New
779 Bidirectional Ammonia Flux Model in an Air Quality Model Coupled With an
780 Agricultural Model, *J. Adv. Model. Earth Syst.*, 11(9), 2934–2957,
781 doi:10.1029/2019MS001728, 2019.
- 782 Putman, W. M. and Lin, S. J.: Finite-volume transport on various cubed-sphere grids, *J.*



- 783 Comput. Phys., 227(1), 55–78, doi:10.1016/j.jcp.2007.07.022, 2007.
- 784 Pye, H. O., Luecken, D. J., Xu, L., Boyd, C. M., Ng, N. L., Baker, K. R., Ayres, B. R.,
785 Bash, J. O., Baumann, K., Carter, W. P., Edgerton, E., Fry, J. L., Hutzell, W. T.,
786 Schwede, D. B. and Shepson, P. B.: Modeling the Current and Future Roles of
787 Particulate Organic Nitrates in the Southeastern United States, *Env. Sci Technol*,
788 49(24), 14195–14203, doi:10.1021/acs.est.5b03738, 2015.
- 789 Pye, H. O. T., Pinder, R. W., Piletic, I. R., Xie, Y., Capps, S. L., Lin, Y. H., Surratt, J. D.,
790 Zhang, Z. F., Gold, A., Luecken, D. J., Hutzell, W. T., Jaoui, M., Offenberg, J. H.,
791 Kleindienst, T. E., Lewandowski, M. and Edney, E. O.: Epoxide Pathways Improve
792 Model Predictions of Isoprene Markers and Reveal Key Role of Acidity in Aerosol
793 Formation, *Env. Sci Technol*, 47(19), 11056–11064, doi:10.1021/es402106h, 2013.
- 794 Pye, H. O. T., Murphy, B. N., Xu, L., Ng, N. L., Carlton, A. G., Guo, H., Weber, R.,
795 Vasilakos, P., Wyatt Appel, K., Hapsari Budisulistiorini, S., Surratt, J. D., Nenes, A.,
796 Hu, W., Jimenez, J. L., Isaacman-Vanwertz, G., Misztal, P. K. and Goldstein, A. H.:
797 On the implications of aerosol liquid water and phase separation for organic aerosol
798 mass, *Atmos. Chem. Phys.*, 17(1), 343–369, doi:10.5194/acp-17-343-2017, 2017.
- 799 Pye, H. O. T., Zuend, A., Fry, J. L., Isaacman-VanWertz, G., Capps, S. L., Appel, K. W.,
800 Foroutan, H., Xu, L., Ng, N. L. and Goldstein, A. H.: Coupling of organic and
801 inorganic aerosol systems and the effect on gas–particle partitioning in



- 802 the southeastern US, *Atmos. Chem. Phys.*, 18(1), 357–370,
803 doi:10.5194/acp-18-357-2018, 2018.
- 804 Pye, H. O. T., D’Ambro, E. L., Lee, B. H., Schobesberger, S., Takeuchi, M., Zhao, Y.,
805 Lopez-Hilfiker, F., Liu, J., Shilling, J. E., Xing, J., Mathur, R., Middlebrook, A. M.,
806 Liao, J., Welti, A., Graus, M., Warneke, C., de Gouw, J. A., Holloway, J. S., Ryerson,
807 T. B., Pollack, I. B. and Thornton, J. A.: Anthropogenic enhancements to production
808 of highly oxygenated molecules from autoxidation, *Proc. Natl. Acad. Sci. U. S. A.*,
809 116(14), 6641–6646, doi:10.1073/pnas.1810774116, 2019.
- 810 Ryan, W. F.: The air quality forecast rote: Recent changes and future challenges, *J. Air*
811 *Waste Manage. Assoc.*, 66(6), 576–596, doi:10.1080/10962247.2016.1151469, 2016.
- 812 Sarwar, G., Fahey, K., Napelenok, S., Roselle, S. and Mathur, R.: Examining the impact
813 of CMAQ model updates on aerosol sulfate predictions, the 10th Annual CMAS
814 Models-3 User's Conference, Chapel Hill, NC, October 2011, 2011.
- 815 Sarwar, G., Simon, H., Bhave, P. and Yarwood, G.: Examining the impact of
816 heterogeneous nitryl chloride production on air quality across the United States,
817 *Atmos. Chem. Phys.*, 12(14), 6455–6473, doi:10.5194/acp-12-6455-2012, 2012.
- 818 Sarwar, G., Gantt, B., Schwede, D., Foley, K., Mathur, R. and Saiz-Lopez, A.: Impact of
819 Enhanced Ozone Deposition and Halogen Chemistry on Tropospheric Ozone over
820 the Northern Hemisphere, *Environ. Sci. Technol.*, 49(15), 9203–9211,



- 821 doi:10.1021/acs.est.5b01657, 2015.
- 822 Schwede, D., Pouliot, G. and Pierce, T.: CHANGES TO THE BIOGENIC EMISSIONS
823 INVENTORY SYSTEM VERSION 3 (BEIS3). [online] Available from:
824 https://www.cmascenter.org/conference/2005/abstracts/2_7.pdf (Accessed 28 June
825 2020), 2005.
- 826 Shen, L., Mickley, L. J. and Gilleland, E.: Impact of increasing heat waves on U.S. ozone
827 episodes in the 2050s: Results from a multimodel analysis using extreme value
828 theory, *Geophys. Res. Lett.*, 43(8), 4017–4025, doi:10.1002/2016GL068432, 2016.
- 829 Sillman, S.: The relation between ozone, NO(x) and hydrocarbons in urban and polluted
830 rural environments, *Atmos. Environ.*, 33(12), 1821–1845,
831 doi:10.1016/S1352-2310(98)00345-8, 1999.
- 832 Sillman, S. and Samson, P. J.: Impact of temperature on oxidant photochemistry in urban
833 polluted rural and remote environments, *J. Geophys. Res.*, 100(D6), 11497–11508,
834 doi:10.1029/94jd02146, 1995.
- 835 Simon, H., and Bhawe, P. V.: Simulating the degree of oxidation in atmospheric organic
836 particles. *Environmental Science and Technology*, 46(1), 331–339.
837 <https://doi.org/10.1021/es202361w>, 2012.
- 838 Stajner, I., Davidson, P., Byun, D., McQueen, J., Draxler, R., Dickerson, P. and Meagher,
839 J.: US National Air Quality Forecast Capability: Expanding Coverage to Include



- 840 Particulate Matter, in Air Pollution Modeling and its Application XXI, pp. 379–384,
841 Springer, Dordrecht., 2011.
- 842 Stein, A. F., Lamb, D. and Draxler, R. R.: Incorporation of detailed chemistry into a
843 three-dimensional Lagrangian-Eulerian hybrid model: Application to regional
844 tropospheric ozone, *Atmos. Environ.*, 34(25), 4361–4372,
845 doi:10.1016/S1352-2310(00)00204-1, 2000.
- 846 Taylor, K. E.: Summarizing multiple aspects of model performance in a single diagram, *J.*
847 *Geophys. Res. Atmos.*, 106(D7), 7183–7192, doi:10.1029/2000JD900719, 2001.
- 848 Tegtmeier, S., Ziska, F., Pisso, I., Quack, B., Velders, G. J. M., Yang, X. and Krüger, K.:
849 Oceanic bromoform emissions weighted by their ozone depletion potential, *Atmos.*
850 *Chem. Phys.*, 15(23), 13647–13663, doi:10.5194/acp-15-13647-2015, 2015.
- 851 United States Environmental Protection Agency: CMAQ (Version 5.02) [Software].
852 Available from <https://zenodo.org/record/1079898>, 2014.
- 853 Wang, K., Yahya, K., Zhang, Y., Hogrefe, C., Pouliot, G., Knote, C., Hodzic, A., San
854 Jose, R., Perez, J. L., Jiménez-Guerrero, P., Baro, R., Makar, P. and Bennartz, R.: A
855 multi-model assessment for the 2006 and 2010 simulations under the Air Quality
856 Model Evaluation International Initiative (AQMEII) Phase 2 over North America:
857 Part II. Evaluation of column variable predictions using satellite data, *Atmos.*
858 *Environ.*, 115, 587–603, doi:10.1016/j.atmosenv.2014.07.044, 2015.



- 859 Watanabe, K.: Measurements of ozone concentrations on a commercial vessel in the
860 marine boundary layer over the northern North Pacific Ocean, *J. Geophys. Res.*,
861 110(D11), D11310, doi:10.1029/2004JD005514, 2005.
- 862 Xu, L., Pye, H. O. T., He, J., Chen, Y., Murphy, B. N. and Ng, N. L.: Experimental and
863 model estimates of the contributions from biogenic monoterpenes and sesquiterpenes
864 to secondary organic aerosol in the southeastern United States, *Atmos. Chem. Phys.*,
865 18(17), 12613–12637, doi:10.5194/acp-18-12613-2018, 2018.
- 866 Yang, F.: GDAS/GFS V15.0.0 Upgrades for Q2FY2019, Retrieved from
867 [https://www.emc.ncep.noaa.gov/users/Alicia.Bentley/fv3gfs/updates/EMC_CCB_FV3GFS_](https://www.emc.ncep.noaa.gov/users/Alicia.Bentley/fv3gfs/updates/EMC_CCB_FV3GFS_9-24-18.pdf)
868 [9-24-18.pdf](https://www.emc.ncep.noaa.gov/users/Alicia.Bentley/fv3gfs/updates/EMC_CCB_FV3GFS_9-24-18.pdf), last access: May 2020, 2019.
- 869 Yang, X., Blechschmidt, A.-M., Bognar, K., McClure–Begley, A., Morris, S.,
870 Petropavlovskikh, I., Richter, A., Skov, H., Strong, K., Tarasick, D., Uttal, T.,
871 Vestenius, M. and Zhao, X.: Pan-Arctic surface ozone: modelling vs measurements,
872 *Atmos. Chem. Phys. Discuss.*, 1–33, doi:10.5194/acp-2019-984, 2020.
- 873 Yarwood, G., Rao, S., Yocke, M. and Whitten, G.: Updates to the Carbon Bond Chemical
874 Mechanism: CB05. Final Report to the US EPA, RT-0400675. Yocke and Company,
875 Novato, CA, 2005.
- 876 Yarwood, G., Whitten, G.Z., Jung, J., Heo, G. and Allen, D.T.: Development, evaluation
877 and testing of version 6 of the Carbon Bond chemical mechanism (CB6), Final report



- 878 to the Texas Commission on Environmental Quality, Work Order No.
879 582-7-84005-FY10-26, 2010.
- 880 Žabkar, R., Honzak, L., Skok, G., Forkel, R., Rakovec, J., Cegljar, A. and Žagar, N.:
881 Evaluation of the high resolution WRF-Chem (v3.4.1) air quality forecast and its
882 comparison with statistical ozone predictions, *Geosci. Model Dev*, 8, 2119–2137,
883 doi:10.5194/gmd-8-2119-2015, 2015.
- 884 Zhang, C., Xue, M., Supinie, T. A., Kong, F., Snook, N., Thomas, K. W., Brewster, K.,
885 Jung, Y., Harris, L. M. and Lin, S.: How Well Does an FV3-Based Model Predict
886 Precipitation at a Convection-Allowing Resolution? Results From CAPS Forecasts
887 for the 2018 NOAA Hazardous Weather Test Bed With Different Physics
888 Combinations, *Geophys. Res. Lett.*, 46(6), 3523–3531, doi:10.1029/2018GL081702,
889 2019a.
- 890 Zhang, X., Kondragunta, S., Da Silva, A., Lu, S., Ding, H., Li, F. and Zhu, Y.: THE
891 BLENDED GLOBAL BIOMASS BURNING EMISSIONS PRODUCT FROM
892 MODIS AND VIIRS Observations (GBBEPx). [online] Available from:
893 https://www.ospo.noaa.gov/Products/land/gbbepx/docs/GBBEPx_ATBD.pdf
894 (Accessed 28 June 2020b), 2019.
- 895 Zhang, Y., Liu, P., Pun, B. and Seigneur, C.: A comprehensive performance evaluation of
896 MM5-CMAQ for the Summer 1999 Southern Oxidants Study episode—Part I:



- 897 Evaluation protocols, databases, and meteorological predictions, *Atmos. Environ.*,
898 40(26), 4825–4838, doi:10.1016/j.atmosenv.2005.12.043, 2006.
- 899 Zhang, Y., Vijayaraghavan, K., Wen, X.-Y., Snell, H. E. and Jacobson, M. Z.: Probing
900 into regional ozone and particulate matter pollution in the United States: 1. A 1 year
901 CMAQ simulation and evaluation using surface and satellite data, *J. Geophys. Res.*,
902 114(D22), D22304, doi:10.1029/2009JD011898, 2009.
- 903 Zhang, Y., Bocquet, M., Mallet, V., Seigneur, C. and Baklanov, A.: Real-time air quality
904 forecasting, part I: History, techniques, and current status, *Atmos. Environ.*, 60,
905 632–655, doi:10.1016/j.atmosenv.2012.06.031, 2012a.
- 906 Zhang, Y., Bocquet, M., Mallet, V., Seigneur, C. and Baklanov, A.: Real-time air quality
907 forecasting, Part II: State of the science, current research needs, and future prospects,
908 *Atmos. Environ.*, 60, 656–676, doi:10.1016/j.atmosenv.2012.02.041, 2012b.
- 909 Zhang, Y., Hong, C., Yahya, K., Li, Q., Zhang, Q. and He, K.: Comprehensive evaluation
910 of multi-year real-time air quality forecasting using an online-coupled
911 meteorology-chemistry model over southeastern United States, *Atmos. Environ.*, 138,
912 162–182, doi:10.1016/j.atmosenv.2016.05.006, 2016.
- 913 Zhang, Y., Jena, C., Wang, K., Paton-Walsh, C., Guérette, É.-A., Utembe, S., Silver, J. D.
914 and Keywood, and M.: Multiscale Applications of Two Online-Coupled
915 Meteorology-Chemistry Models during Recent Field Campaigns in Australia, Part I:



- 916 Model Description and WRF/Chem-ROMS Evaluation Using Surface and Satellite
917 Data and Sensitivity to Spatial Grid Resolutions, *Atmosphere (Basel)*, 10(4), 189,
918 doi:10.3390/atmos10040189, 2019c.
- 919 Zhang, Y., Wang, K., Jena, C., Paton-Walsh, C., Guérette, É. A., Utembe, S., Silver, J. D.
920 and Keywood, M.: Multiscale applications of two online-coupled
921 meteorology-chemistry models during recent field campaigns in Australia, Part II:
922 Comparison of WRF/Chem and WRF/Chem-ROMS and impacts of air-sea
923 interactions and boundary conditions, *Atmosphere (Basel)*, 10(4), 210,
924 doi:10.3390/ATMOS10040210, 2019d.
- 925 Zhu, Y. and Luo, Y.: Precipitation Calibration Based on the Frequency-Matching Method,
926 *Weather Forecast.*, 30(5), 1109–1124, doi:10.1175/WAF-D-13-00049.1, 2015.
- 927



Tables and Figures

Table 1. Configuration of GFSv15-CMAQv5.0.2 system

Attribute	Model Configuration
Forecast period	Jan.-Dec., 2019
Domain	Continental U.S.
Resolution	Horizontal: 12 km (442×265); Vertical: 35 layers
Physical Options	
Shortwave/longwave radiation	The Rapid Radiative Transfer Method for GCMs
Planetary boundary layer (PBL)	Hybrid eddy-diffusivity mass-flux (EDMF) PBL
Land surface	Noah Land Surface Model (LSM)
Microphysics	A more advanced GFDL microphysics scheme
Cumulus	The Simplified Arakawa-Schubert (SAS) deep convection
Chemical Options	
Photolysis	In-line method (Binkowski et al., 2007)
Gas-phase chemistry	The Carbon Bond mechanism version 5 with active chlorine chemistry and updated toluene mechanism (CB05tucl) (Yarwood et al., 2005; Sarwar et al., 2012)
Aqueous-phase chemistry	AQCHEM (Sarwar et al., 2011)
Aerosol module	AERO6 with nonvolatile POA (Carlton et al., 2010; Simon et al., 2012; Appel et al., 2013)

Table 2. Performance statistics of meteorological forecasts

Datasets		CASTNET							METAR						
Variable	Period	Mean Obs.	Mean Sim.	MB	RMSE	NMB, NME, %		Corr	Mean Obs.	Mean Sim.	MB	RMSE	NMB, NME, %		Corr
T2, °C	DJF	-0.1	-0.5	-0.4	2.6	-588	-2850	0.96	2.7	2.6	-0.1	2.5	-3.1	69.3	0.97
	MAM	9.9	9.4	-0.5	2.4	-5.2	18.2	0.97	12.3	11.9	-0.4	2.3	-3.0	14.0	0.97
	JJA	21.5	21.4	-0.2	2.4	-0.8	8.6	0.93	23.4	23.1	-0.3	2.3	-1.2	7.5	0.93
	SON	11.5	11.3	-0.2	2.6	-2.0	16.1	0.97	13.8	13.8	0.1	2.3	0.4	12.6	0.98
	Annual	10.9	10.6	-0.3	2.5	-3.0	17.0	0.98	13.2	13.0	-0.2	2.3	-1.3	13.1	0.98
RH2, %	DJF	69.1	71.9	2.8	14.3	4.0	15.1	0.74	74.1	74.4	0.4	13.3	0.5	13.4	0.76
	MAM	62.7	66.1	3.4	14.2	5.4	16.6	0.82	67.4	70.1	2.7	13.8	4.0	15.5	0.81
	JJA	55.0	53.3	-1.7	12.2	-3.2	16.4	0.89	67.0	67.3	0.3	13.1	0.5	14.8	0.84
	SON	59.0	57.6	-1.4	13.0	-2.4	16.1	0.87	68.7	67.0	-1.7	13.2	-2.5	14.5	0.83



WS10, m s ⁻¹	Annual	61.4	62.2	0.8	13.5	1.3	16.0	0.85	68.8	69.3	0.4	13.2	0.8	14.4	0.83
	DJF	2.5	3.0	0.5	2.0	18.7	56.7	0.59	3.3	3.7	0.4	2.0	10.8	43.5	0.71
	MAM	2.8	3.4	0.6	2.1	22.2	55.6	0.60	3.6	4.0	0.4	2.0	10.3	42.5	0.71
	JJA	2.4	3.0	0.6	1.9	24.5	60.9	0.51	2.8	3.3	0.5	1.9	17.0	52.6	0.62
	SON	2.6	3.1	0.5	2.0	20.4	58.6	0.57	4.0	4.1	0.2	1.8	4.2	33.1	0.69
WD10, degree	Annual	2.6	3.1	0.6	2.0	21.5	57.9	0.57	3.4	3.7	0.4	1.9	10.7	41.8	0.72
	DJF	187.2	189.4	2.2	69.4	1.2	26.4	0.81	158.0	164.3	6.4	60.7	4.0	25.5	0.90
	MAM	184.6	186.5	1.9	68.1	1.0	26.1	0.81	159.9	163.6	3.7	60.7	2.3	25.4	0.89
	JJA	186.7	188.8	2.1	73.0	1.1	28.5	0.77	146.8	147.8	1.0	69.9	0.7	33.9	0.86
	SON	181.8	183.9	2.1	71.3	1.1	28.1	0.79	190.9	196.6	5.7	42.1	3.0	14.5	0.92
Precip, mm hr ⁻¹	Annual	185.0	187.1	2.1	70.5	1.1	27.3	0.80	162.5	166.6	4.1	59.1	2.5	23.9	0.89
	DJF	1.0	0.6	-0.4	1.7	-42.5	86.1	0.26	1.3	0.7	-0.6	3.5	-44.4	77.4	0.15
	MAM	1.1	0.6	-0.6	2.0	-51.1	86.3	0.22	1.8	0.7	-1.0	7.5	-58.6	85.6	0.07
	JJA	2.2	0.5	-1.7	4.7	-77.8	93.9	0.11	2.6	0.7	-1.9	7.6	-74.5	91.6	0.04
	SON	1.3	0.6	-0.7	2.4	-54.4	86.2	0.24	1.8	0.8	-1.0	8.8	-56.4	83.8	0.07
Annual	1.3	0.6	-0.7	2.5	-55.4	87.9	0.18	1.8	0.7	-1.1	7.0	-59.1	85.0	0.07	

T2: temperature at 2-m; RH2: relative humidity at 2-m; WS10: wind speed at 10-m; WD10: wind direction

at 10-m; Precip: precipitation; DJF: winter; MAM: spring; JJA: summer; SON: autumn; MB: mean bias;

RMSE: root mean square error; NMB: normalized mean bias; NME: normalized mean error; Corr:

correlation coefficient; Obs.: Observation; Sim.: Prediction.

Table 3. Performance statistics of chemical variables against AIRNow dataset

Period	MDA8 O ₃ , ppb							24-h avg PM _{2.5} , µg m ⁻³							
	Mean Obs.	Mean Sim.	MB	RMSE	NMB,%	NME,%	Corr	Period	Mean Obs.	Mean Sim.	MB	RMSE	NMB,%	NME,%	Corr
Jan	32.4	32.0	-0.3	7.9	-1.1	18.0	0.52	Jan	8.3	13.8	5.5	11.4	66.4	92.4	0.34
Feb	36.7	35.7	-1.1	8.4	-2.9	17.4	0.53	Feb	8.0	12.5	4.5	10.0	55.9	81.0	0.51
Mar	45.1	40.4	-4.7	8.9	-10.4	16.0	0.55	Mar	7.9	11.0	3.1	9.4	39.6	68.9	0.38
Apr	46.6	43.1	-3.5	8.0	-7.5	13.5	0.61	Apr	6.3	8.0	1.7	6.6	26.5	62.0	0.30
May	44.3	42.7	-1.6	7.9	-3.7	14.0	0.66	May	6.8	6.9	0.2	5.0	2.3	49.8	0.23
Jun	45.9	43.9	-2.0	11.2	-4.4	18.5	0.58	Jun	7.2	6.8	-0.4	5.6	-5.1	47.4	0.20
Jul	44.5	46.6	2.1	9.7	4.7	16.7	0.70	Jul	8.3	8.5	0.1	11.7	1.7	59.9	0.30
Aug	43.9	46.9	3.0	9.5	6.8	16.3	0.73	Aug	7.3	6.9	-0.4	4.1	-5.2	40.4	0.33



Sept	42.7	45.6	2.9	8.1	6.8	14.5	0.78	Sept	7.0	7.6	0.5	4.7	7.6	44.4	0.48
Oct	37.2	40.2	3.1	8.0	8.3	15.8	0.77	Oct	6.7	9.5	2.8	8.6	41.7	71.9	0.35
Nov	34.3	34.8	0.5	8.4	1.6	16.9	0.64	Nov	9.0	13.2	4.2	9.8	46.7	72.0	0.48
Dec	30.7	31.2	0.5	9.0	1.6	20.5	0.49	Dec	8.8	13.8	5.0	11.0	56.6	82.9	0.49
O ₃ -season	44.3	45.1	0.9	9.4	2.0	16.0	0.67	DJF	8.4	13.4	5.0	10.8	59.7	85.6	0.45
Non								MAM	7.0	8.6	1.6	7.2	23.5	60.6	0.33
O ₃ -season	38.2	37.4	-0.9	8.4	-2.3	16.4	0.68	JJA	7.6	7.4	-0.2	7.9	-2.6	49.7	0.26
Non								SON	7.5	10.0	2.5	8.0	33.0	63.4	0.45
Annual	41.1	41.0	-0.1	8.9	-0.1	16.2	0.70	Annual	7.6	9.8	2.2	8.6	29.0	65.3	0.40

MDA8 O₃: maximum daily average 8-h ozone; 24-h avg PM_{2.5}: 24-hour average PM_{2.5}.

Figures

Figure 1. Spatial distribution of MBs for forecasted seasonal T2 by GFSv15-CMAQv5.0.2 against observations from METAR

Figure 2. Taylor diagram with variance, Corr, and NMB for meteorological variables (T2, RH2, WS10, WD10, and Precip) against CASTNET and METAR dataset

Figure 3. Spatial distribution of forecasted MDA8, MB, and NMB during O₃ and winter season. Observation from AIRNow is shown as filled circles in the overlay plots of concentrations

Figure 4. Forecasted seasonal daily PM_{2.5} by GFSv15-CMAQv5.0.2 overlaid observations from AIRNow and MB against observations from AIRNow

Figure 5. Categorical evaluation of MDA8 and 24-h avg PM_{2.5}



Figure 6. Monthly AOD from MODIS (left), predicted AOD from GFSv15-CMAQv5.0.2 (middle), and predicted surface 24-h avg $PM_{2.5}$ (right)

Figure 7. Monthly average concentrations of $PM_{2.5}$ components

Figure 8. Annual performance of MDA8 in 10 CONUS regions (a); Taylor Diagram for annual performance of MDA8 (b); Annual performance of 24-h avg $PM_{2.5}$ in 10 CONUS regions (c); Taylor Diagram for annual performance of 24-h avg $PM_{2.5}$. Outliers represent regions with NSDs >3.5 (d)

Figure 9. Diurnal $PM_{2.5}$ in: (a) O_3 season for regions 1 to 5; (b) Non- O_3 season for regions 1 to 5; (c) O_3 season for regions 6 to 10; (d) Non- O_3 season for region 6 to 10.

Solid curves are observed values and dash curves are predicted values. Average of predicted $PM_{2.5}$ and components of $PM_{2.5}$ within CONUS in: (e) O_3 season, and (f) Non- O_3 season

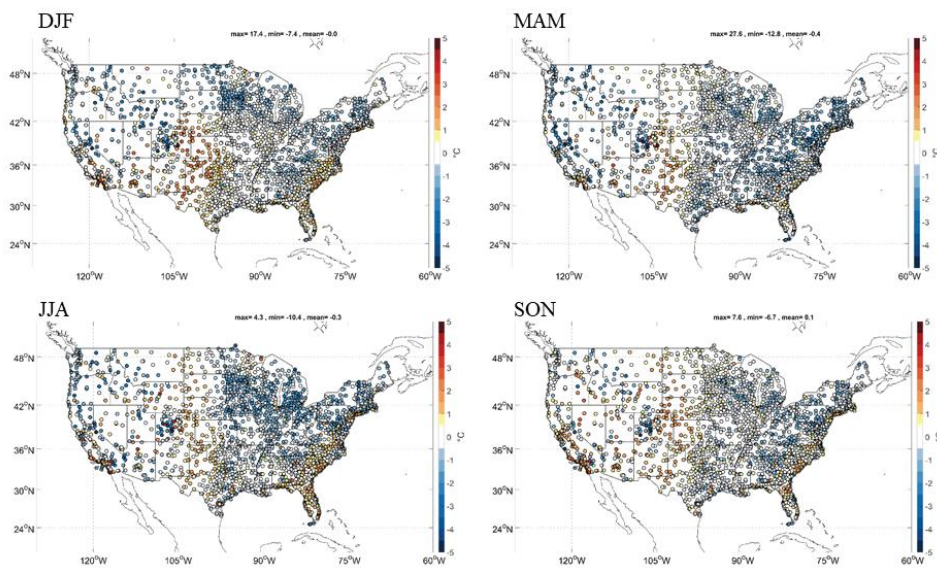


Figure 1. Spatial distribution of MBs for forecasted seasonal mean T2 by

GFSv15-CMAQv5.0.2 against observations from METAR



Annual Performance of MET fields from GFSv15-CMAQv502

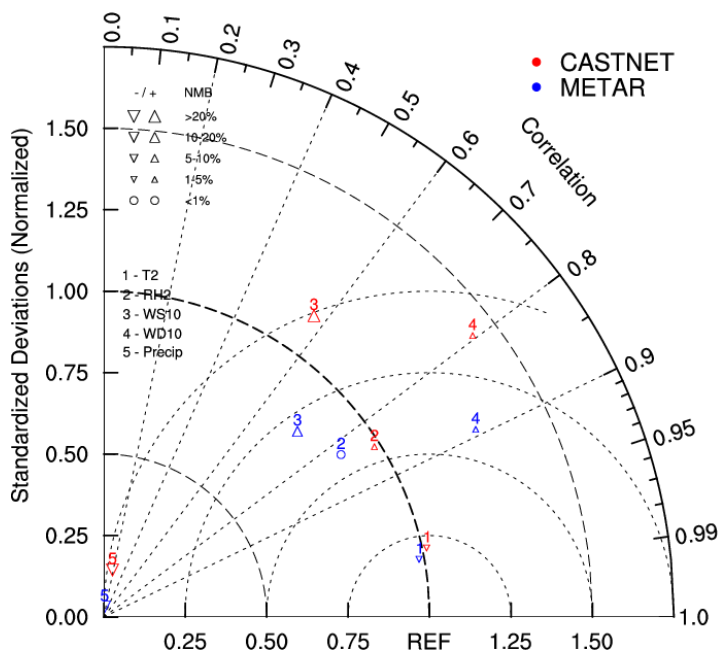


Figure 2. Taylor diagram (Taylor, 2001) with Normalized Standardized Deviations (NSD), Corr, and NMB for meteorological variables (T2, RH2, WS10, WD10, and Precip) against CASTNET and METAR dataset. The REF marker at x-axis represents a referred perfect performance. The closer each variable is to the REF marker, the better performance the forecast system has for that variable

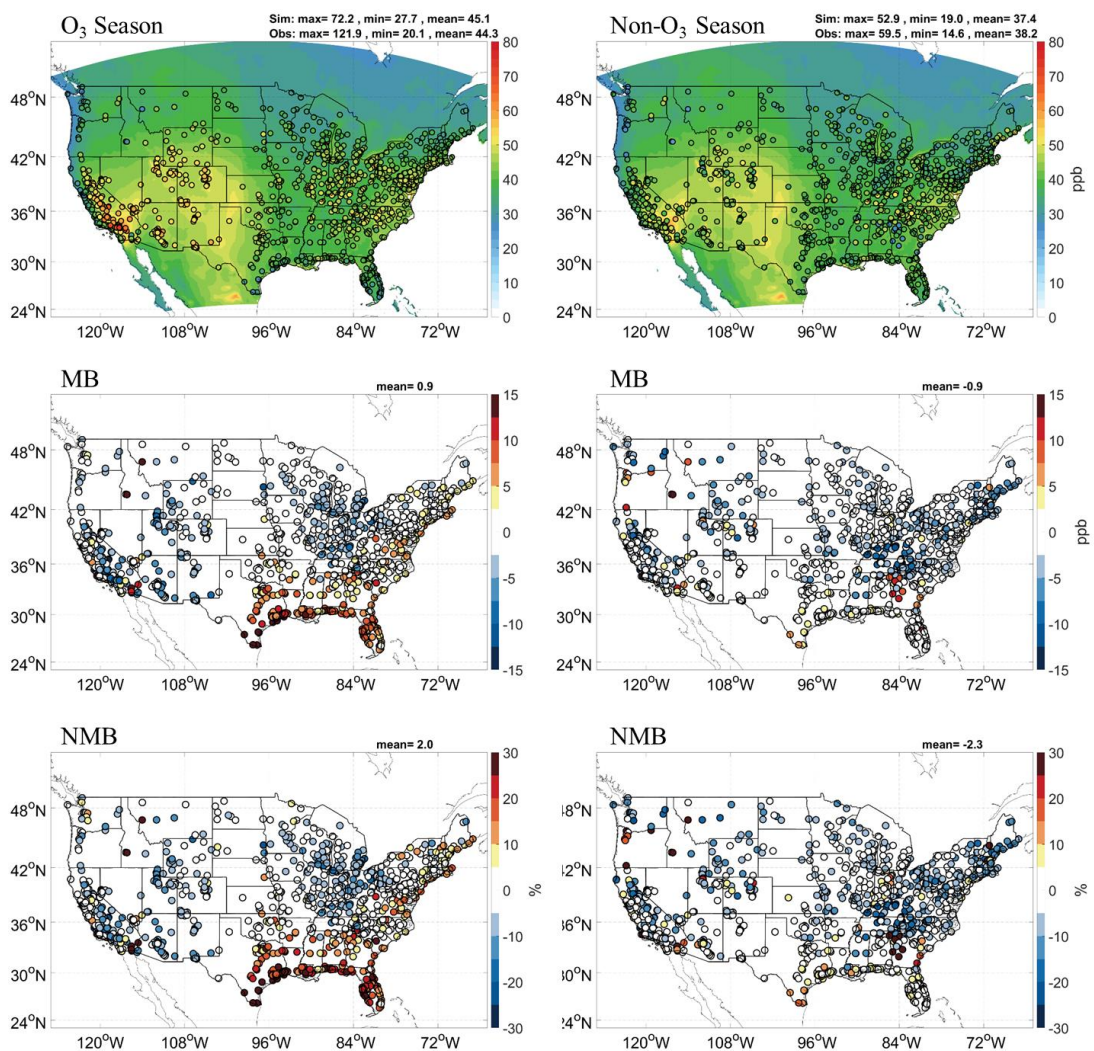


Figure 3. Spatial distribution of forecasted MDA8, MB, and NMB during O₃ and non-O₃ season. Observation from AIRNow is shown as filled circles in the overlay plots of concentrations

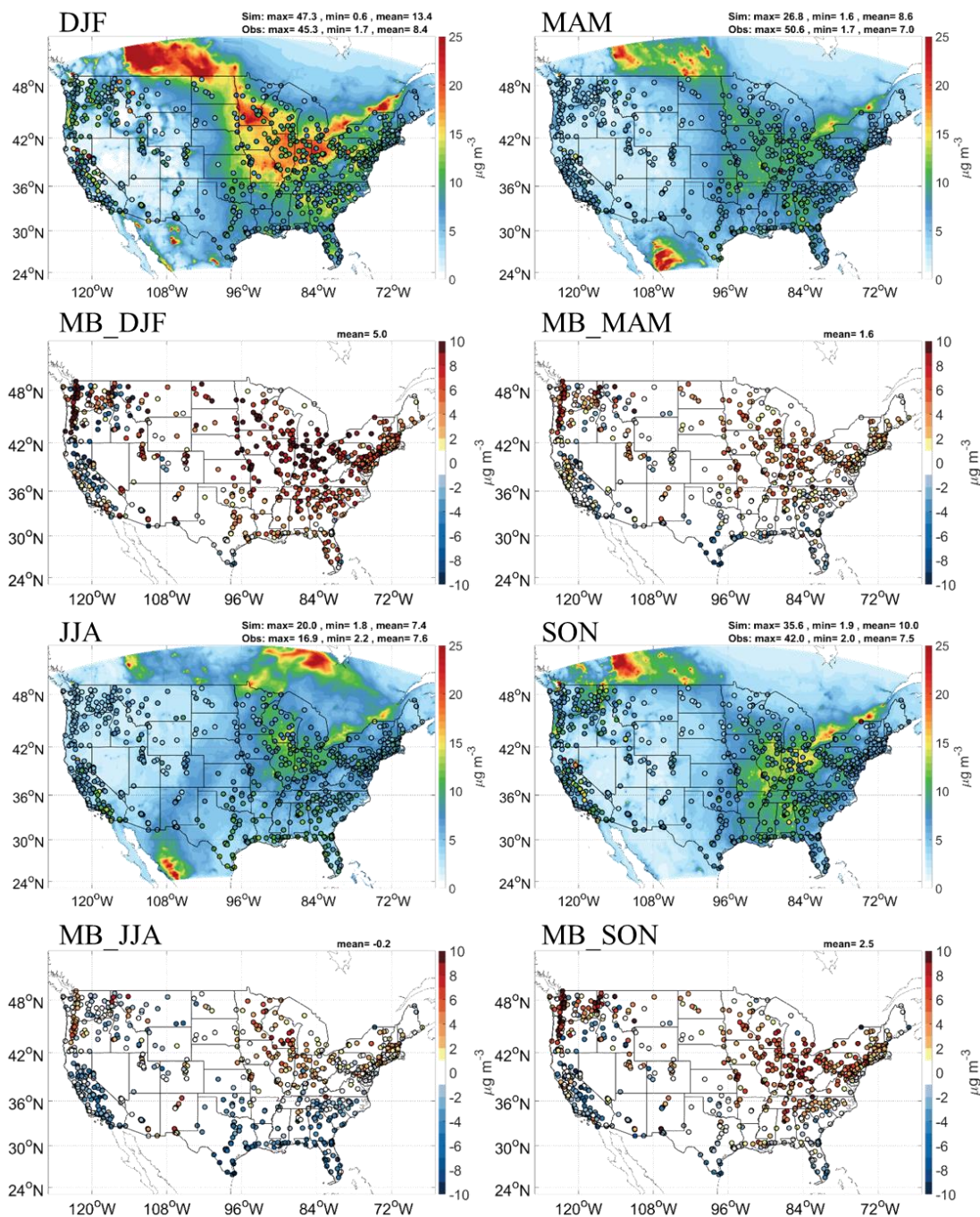




Figure 4. Forecasted seasonal daily $PM_{2.5}$ by GFSv15-CMAQv5.0.2 overlaid observations from AIRNow and MB against observations from AIRNow

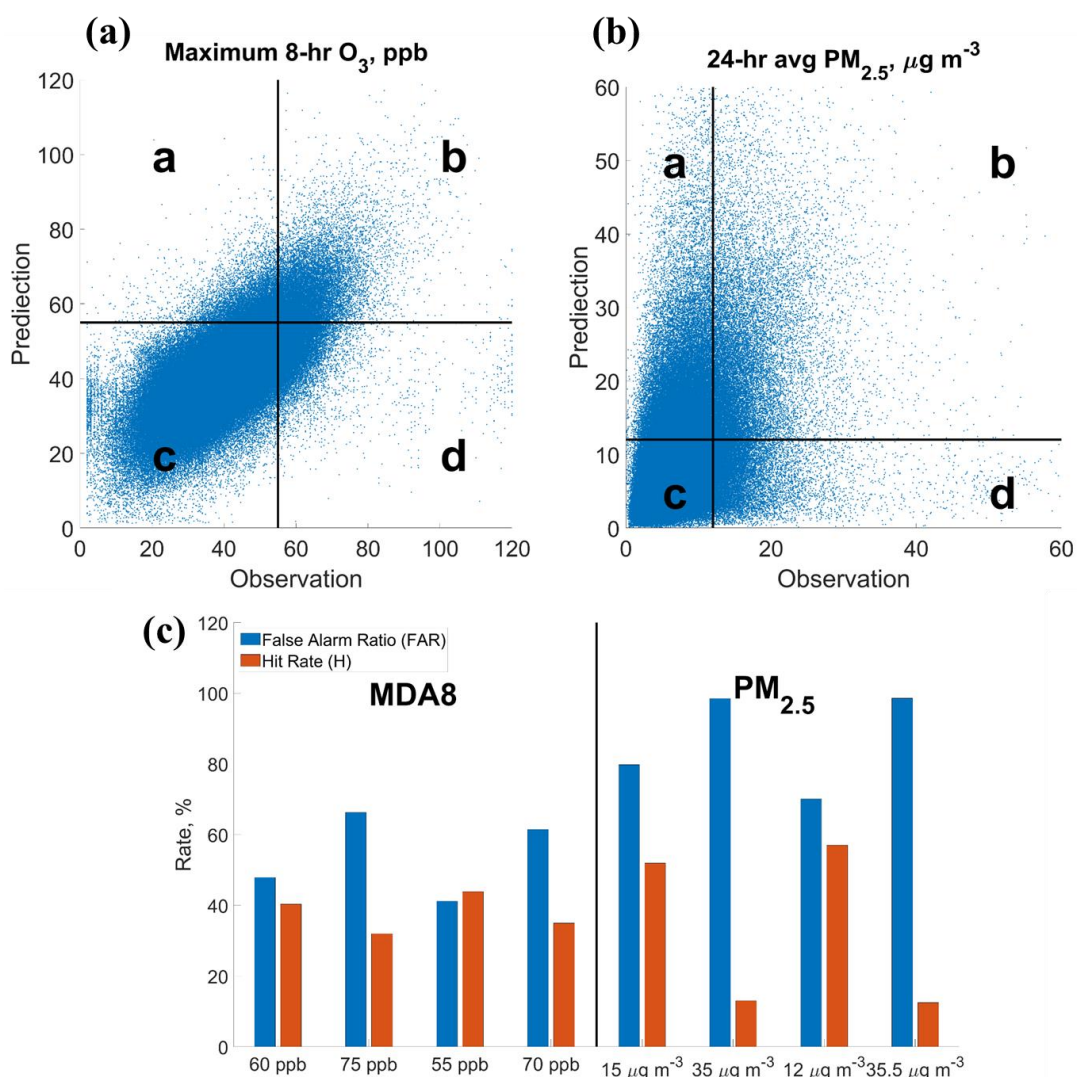




Figure 5. Categorical evaluation of MDA8 and 24-h avg $PM_{2.5}$: (a) scatter plot of predicted and observed MDA8. The scatters are categorized into 4 areas using the threshold of 55 ppb for both observation and prediction; (b) scatter plot of predicted and observed 24-h avg $PM_{2.5}$. The scatters are categorized into 4 areas using the threshold of $12 \mu\text{g m}^{-3}$ for both observation and prediction; (c) False Alarm Ratio (FAR) and Hit Rate (H) in 4 categories for forecasts of MDA8 and 24-h avg $PM_{2.5}$.

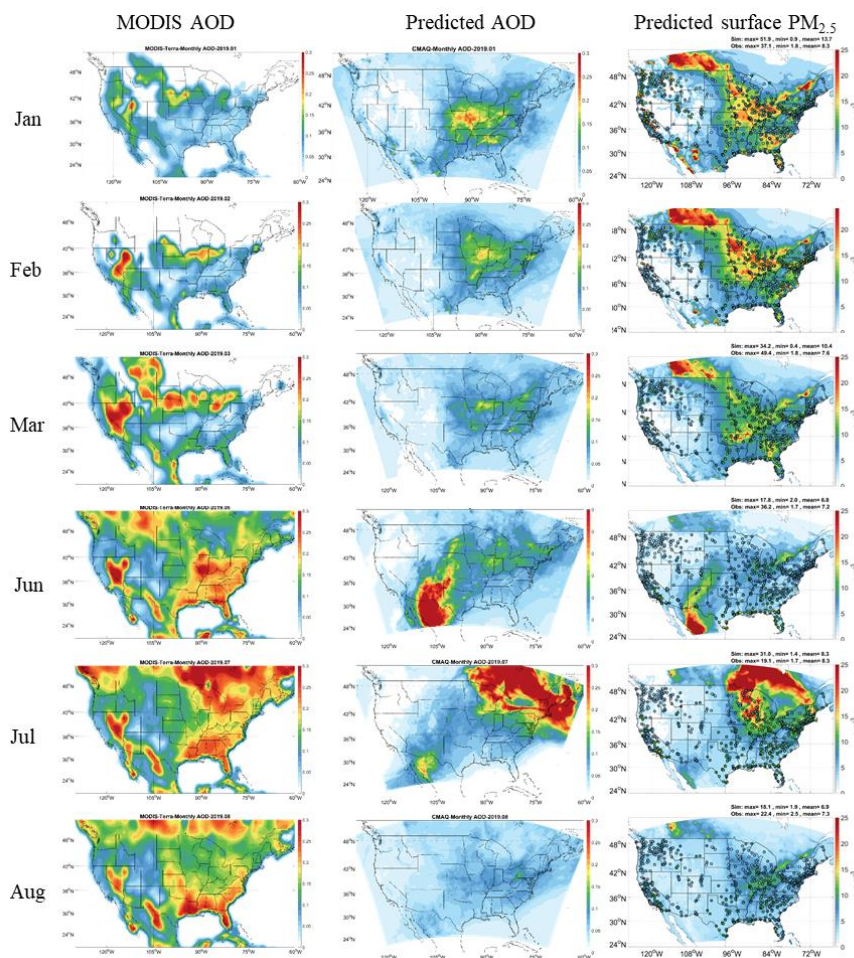


Figure 6. Monthly AOD from MODIS (left), predicted AOD from GFSv15-CMAQv5.0.2 (middle), and predicted surface 24-h avg PM_{2.5} (right)

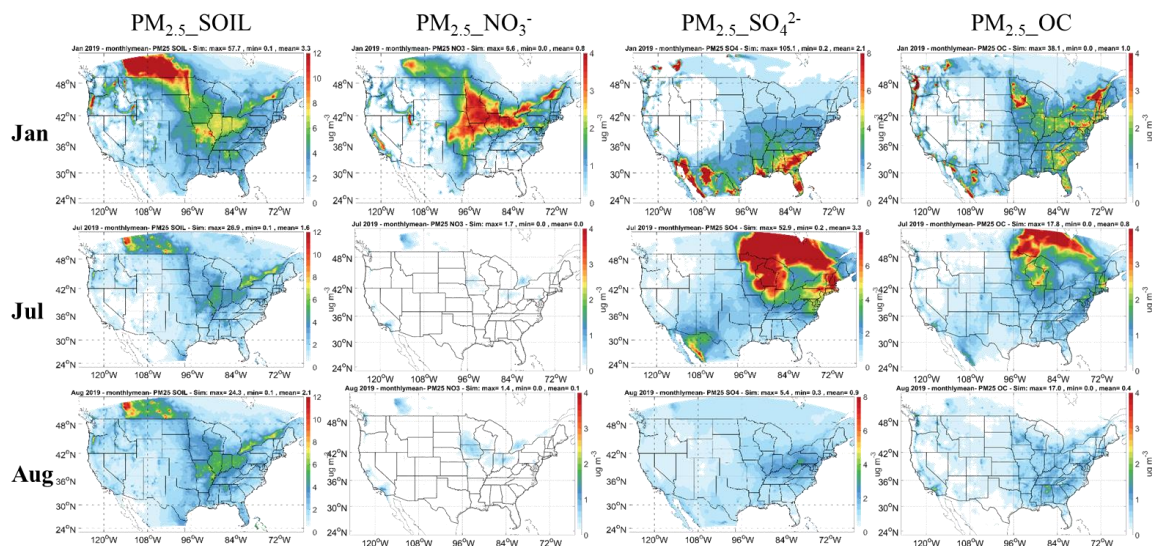


Figure 7. Monthly average concentrations of $PM_{2.5}$ components in Jan, Jul, and Aug.

$PM_{2.5_SOIL}$: soil components and unspecified coarse mode components; $PM_{2.5_NO_3^-}$: nitrate components; $PM_{2.5_SO_4^{2-}}$: sulfate components; $PM_{2.5_OC}$: organic carbon components.

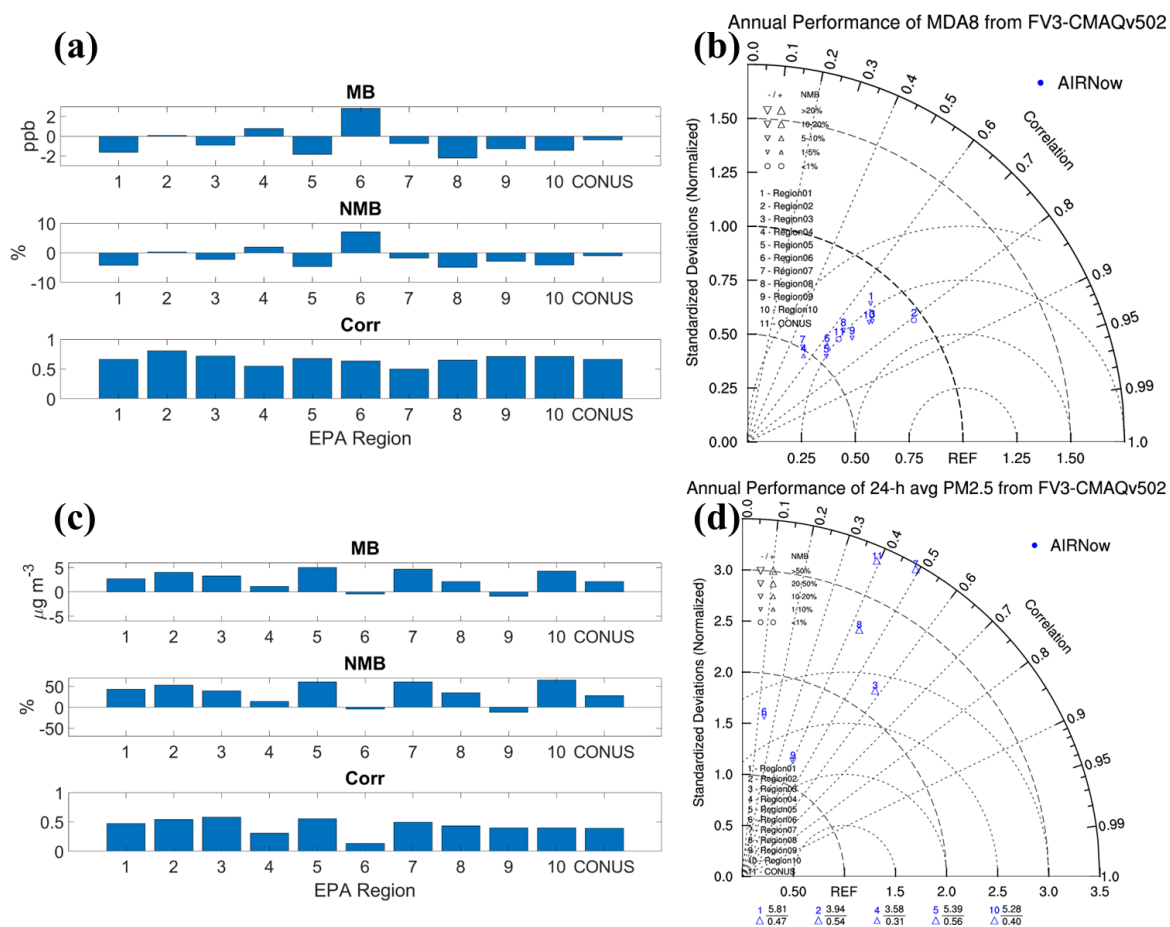


Figure 8. Annual performance of MDA8 in 10 CONUS regions (a); Taylor Diagram for annual performance of MDA8 (b); Annual performance of 24-h avg PM_{2.5} in 10 CONUS regions (c); Taylor Diagram for annual performance of 24-h avg PM_{2.5}. Outliers represent regions with NSDs >3.5 (d)

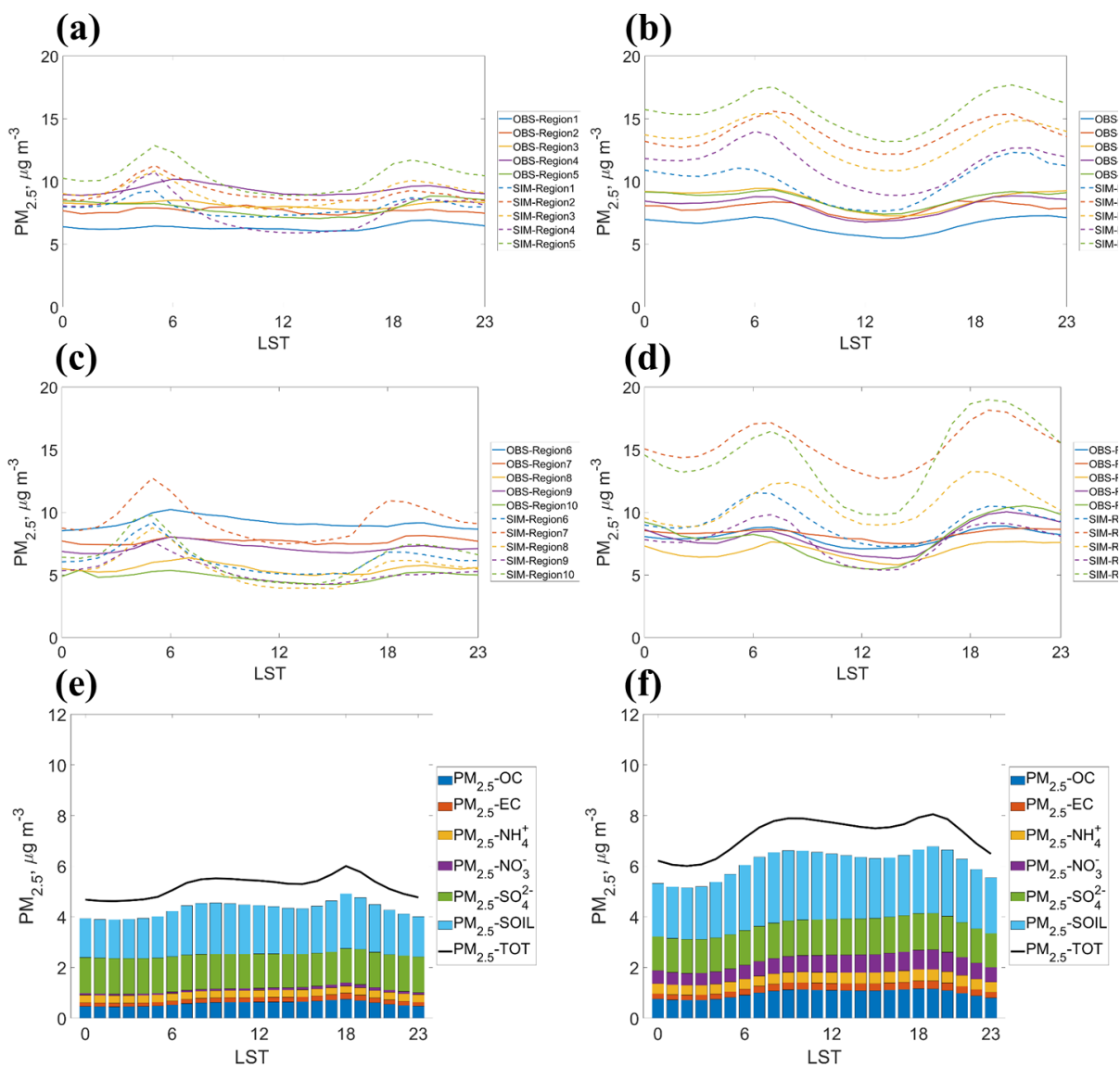


Figure 9. Diurnal PM_{2.5} in: (a) O₃ season for regions 1 to 5; (b) Non-O₃ season for regions 1 to 5; (c) O₃ season for regions 6 to 10; (d) Non-O₃ season for region 6 to 10.

Solid curves are observed values and dash curves are predicted values. Average of



predicted $PM_{2.5}$ and components of $PM_{2.5}$ within CONUS in: (e) O_3 season, and (f)

Non- O_3 season.